Evidence of subduction-related components in sapphirine-bearing gabbroic dykes (Finero phlogopite–peridotite): Insights into the source of the Triassic–Jurassic magmatism at the Europe–Africa boundary / Giovanardi, Tommaso; Zanetti, Alberto; Dallai, Luigi; Morishita, Tomoaki; Hémond, Christophe; Mazzucchelli, Maurizio. - In: LITHOS. - ISSN 0024-4937. - 354–355:(2020), pp. 1-16. [10.1016/j.lithos.2020.105366]

Evidence of subduction-related components in sapphirine-bearing gabbroic dykes (Finero Phlogopite–Peridotite): Insights into the source of the Triassic–Jurassic magmatism at the Europe–Africa boundary

Tommaso Giovanardi[1,2#], Alberto Zanetti[3#], Luigi Dallai[4], Tomoaki Morishita[5], Christophe Hémond[6], Maurizio Mazzucchelli[2]*

[1]DIPARTIMENTO DI SCIENZE DELLA TERRA E DELL'AMBIENTE, UNIVERSITA' DEGLI STUDI DI PAVIA, VIA FERRATA 1, 27100 PAVIA, ITALY

[2]DIPARTIMENTO DI SCIENZE CHIMICHE E GEOLOGICHE, UNIVERSITA' DEGLI STUDI DI MODENA E REGGIO EMILIA, VIA CAMPI 103, 41121 MODENA, ITALY

[3]ISTITUTO DI GEOSCIENZE E GEORISORSE-C.N.R. PAVIA, VIA FERRATA 1, 27100 PAVIA, ITALY

[4]ISTITUTO DI GEOSCIENZE E GEORISORSE-C.N.R. PISA, VIA MORUZZI 1, 56124 PISA, ITALY

[5]FRONTIER SCIENCE ORGANIZATION, KANAZAWA UNIVERSITY, 920-1192 KANAZAWA, JAPAN

[6]LABORATOIRE GÉOSCIENCES OCÉAN, UMR6538, INSTITUT UNIVERSITAIRE EUROPÉEN DE LA MER, UNIVERSITÉ DE BREST & CNRS, PLACE NICOLAS COPERNIC, F-29280, PLOUZANÉ, FRANCE.

# these authors are equal first authors of this work

* Corresponding author: maurizio.mazzucchelli@unimore.it

Keywords: sapphirine; Finero; mantle peridotite; dykes; Ivrea Verbano

Abstract

A gabbroic dyke swarm containing magmatic sapphirine occurs in the Finero phlogopite–peridotite (FPP), one of the major mantle massifs in the Ivrea–Verbano Zone (IVZ; western Southern Alps). Sapphirine is part of a particular mineral assemblage, including plagioclase, titanian pargasite, titanian phlogopite, and Cl-rich apatite; the latter mineral hosts calcite inclusions. The dykes cut the mantle foliation at a high angle, are bounded by orthopyroxenite layers, and show symmetric internal banding, represented by two outer hornblendite selvages and an inner leucogabbro band. The sapphirine occurs in up to 3 cm-thick irregular patches in both hornblendite salvages, along with Al-rich amphibole and green spinel.

We present major and trace elements of minerals and bulk rock, as well as mineral O, Sr, and Nd isotopic compositions of dykes and the host peridotite from two different outcrops in the FPP area. Our data show that early melt migration developed through porous flow within cm-thick channels and was characterised by orthopyroxene dissolution. Following progressive percolation and reaction, the melt became silica saturated with segregation of orthopyroxenite in the centres of the channels. The banded internal structure of the dykes was caused by three different evolutionary stages, involving opening and enlargement of the conduits. The sapphirine and green spinel segregation took place at T > 1,000 °C, in the presence of melt with transient composition, which interstitially migrated and reacted with the cumulus minerals to form the hornblendite layers. The mineral chemistry of the newly-formed amphiboles indicates that the sapphirine parental melt was Al-rich, depleted to strongly depleted in Hf, Zr, Nb, Ta, Ti, Sc, V, and middle and heavy rare earth elements, and characterised by a positive Eu anomaly and $(Zr/Hf)_N < 1$. These data suggest a parental melt with a significant amount of normative plagioclase. However, the studied veins do not show evidence of plagioclase assimilation, and we argue that this process could have occurred in magmatic bodies that are not outcropping today to the surface or in the melt source.

The $\delta^{18}O$ values of vein amphiboles and plagioclases vary from 6.9 to 8.6‰ SMOW, which is well above the mantle range, even when considering fractionation upon cooling. Given that

orthopyroxene from the wall has “normal” mantle $\delta^{18}O$ values (5.8‰), reaction with the host metasomatised peridotite cannot be responsible for the heavy $\delta^{18}O$ signature, and the latter must have been imparted by crustal components deeper in the mantle.

Our petrographic and geochemical evidence demonstrates that the northern IVZ records an extremely prolonged release, from the Variscan orogenic cycle to the Mesozoic exhumation, of K-H_2O-rich mantle-derived melts, mixed with subduction-related components. This finding provides valuable insights into the Triassic–Jurassic magmatism and the geodynamic environment at the Europe–Africa boundary.

1. Introduction

It is well known that the subcontinental lithospheric mantle (SCLM) may record significant heterogeneities in terms of both lithology and geochemical composition, resulting from the development of different tectono-magmatic events over a long time span (Mukasa and Shervais, 1999; Rivalenti et al., 2007a, b; Mazzucchelli et al., 2009; 2010; 2016; Borghini et al., 2017; Princivalle et al., 2014; Ponce et al., 2015; Rocco et al., 2017; Consuma et al., 2019). The petrochemical records of the lithospheric mantle and uprising melts can be very different based on the geochemical affinity of the melt, the composition of the peridotite mantle column, the modalities of melt migration, and the P, T, fO_2, and fH_2 conditions of the system. An exceptional locality where this can be studied in great detail is the phlogopite–peridotite mantle unit of Finero (Cawthorn, 1975; Siena & Coltorti, 1989). The Finero phlogopite–peridotite (FPP) is one of the most studied mantle massifs on Earth. It crops out in the northernmost part of the Ivrea–Verbano Zone (IVZ, western Southern Alps, Italy; Fig. 1) and consists of an association of phlogopite-bearing amphibole harzburgites and dunites, both locally associated with phlogopite-bearing amphibole pyroxenites. This is the result of an important episode of pervasive to channelled porous flow migration of melts containing a large volume of crustal components that induced virtually complete metasomatic recrystallisation of an older sequence of harzburgite and pyroxenite associations (Lensch, 1968; Cawthorn, 1975; Griffin & O'Reilly, 1986; Siena & Coltorti, 1989; Shervais and Musaka, 1991; Hartmann & Wedepohl, 1993; Zanetti et al., 1999, 2016; Grieco et al., 2001, 2004; Morishita et al., 2003, 2008; Raffone et al., 2006; Selverstone & Sharp, 2011; Mazzucchelli et al., 2014; Tommasi et al., 2017). The crustal affinity of these metasomatic melts is implied by high $\delta^{18}O$ values and by the Nd, Sr, Pb, H, S, Cl, and noble gas isotopic compositions of the FPP rocks (Hunziker and Zingg, 1982; Voshage et al., 1987, 1988; Cumming et al., 1987; Hartmann and Wedepohl, 1993; Obermiller, 1994; Seitz and Woodland, 2000; Downes, 2001; Matsumoto et al., 2005; Selverstone and Sharp, 2011). The melt migration processes have been mainly attributed to supra-subduction environments (e.g. Zanetti et al., 1999; Grieco et al., 2001, 2004; Morishita et al., 2003, 2008; Matsumoto et al., 2005), but also to extensional settings (Garuti et al., 2001; Zaccarini et al., 2004).

The available geochronological data indicate that this main event of melt migration took place in the Palaeozoic (Zanetti et al., 2016; Malitch et al., 2017), but many field, petrochemical, and geochronological data point to the development of several other tectono-magmatic events in the Mesozoic as well (Stähle et al., 1990, 2001; Grieco et al., 2001; Matsumoto et al., 2005; Morishita et al., 2003, 2008; Zanetti et al., 1999; 2016; Malitch et al., 2017).

Giovanardi et al. (2013) studied the occurrence of a late sapphirine-bearing gabbroic dykelet swarm previously reported by Siena & Coltorti (1989) and discovered by M. Mazzucchelli (Giovanardi et al., 2013). Based on a detailed petrographic and geochemical survey, they provided evidence for a multi-stage dyke formation, which involved fractional crystallisation associated with different patterns of melt–rock interactions.

With the aim of better constraining the nature of the primitive melt and petrological processes and inducing the segregation of sapphirine in the dykes, in this paper, new and detailed petrochemical data are reported for dykes and host peridotites close to the area studied by Giovanardi et al. (2013) and on a second finding in an adjacent area. Particular care has been dedicated to characterising the compositional variability in terms of major and trace element mineral chemistry, as well as the mineral O, Nd, and Sr isotopic composition, to document the geochemical fractionation of the flowing melt following reaction with the host peridotite and early cumulates. The genetic and temporal relationships between the dyke emplacement and other events of melt migration recorded by the FPP unit, as well as the related geodynamic scenarios, are also addressed.

2. Geological setting

In the Finero area (Fig. 1), the IVZ crops out in a pseudo-antiform structure with the FPP mantle unit at the core, flanked by what has been called the Finero Mafic Complex (Cawthorn, 1975; Siena & Coltorti, 1989; Lu et al., 1997a, b; Zanetti et al., 2013, 2014; Giovanardi et al., 2014; Mazzucchelli et al., 2014; Langone et al., 2017). The Mafic Complex is divided into three different units: the stratigraphically lower Layered Internal Zone unit (LIZ), in contact with the FPP; the Amphibole-Peridotite (Amphibole-Pd); and the External Gabbro (EG). The EG is placed in tectonic contact with the Amphibole-Peridotite by a Mesozoic high-T shear-zone (Langone et al., 2018). A tectonic contact also characterises the transition toward the amphibolite-facies metasediments and metabasites of the Kinzigite Formation (KF), which represent the metamorphic basement of the Adria Plate. Septa of KF rocks are embedded in the EG.

The Finero mafic–ultramafic sequence presents several differences with respect to the southern and central sectors of the IVZ (i.e. the Baldissero and Balmuccia peridotites and the Val Sesia Complex; Quick et at., 1995; Correia et al., 2012; Mazzucchelli et al., 2014 and references therein), providing evidence of a different geological evolution (Zanetti et al., 2013, 2014, 2016; Langone et al., 2017, 2018). In particular, the FPP has been completely recrystallised by several events of migrating melts with crustal affinity (Zanetti et al., 1999; 2016; Mazzucchelli et al., 2014 and references therein), and the relationships with the parental melts of the surrounding Mafic Complex are far from being understood (Giovanardi et al., 2014). Conversely, the peridotites cropping out in the central and southern part of IVZ did not undergo similar melt-induced recrystallisation and were emplaced in the Kinzigite Formation as tectonic slivers before the intrusion of the central and southern Mafic Complex (Quick et at., 1995; Mazzucchelli et al., 2014 and references therein).

The FPP is mainly represented by phlogopite-bearing amphibole harzburgites and associated phlogopite-bearing pyroxenites (Cawthorn, 1975; Siena & Coltorti, 1989; Hartmann & Wedephol, 1993; Zanetti et al., 1999; Raffone et al., 2006; Selverstone & Sharp, 2011; Mazzucchelli et al., 2014; Giovanardi et al., 2018). These lithologies derived from pervasive metasomatism of a depleted peridotite, which formed secondary orthopyroxene, amphibole, and phlogopite (Zanetti et al., 1999; Tommasi et al., 2017). Channelled migration events formed dunite bodies containing stratiform to podiform chromitites and, rarely, pyroxenite and hornblendite layers (Grieco et al., 2001, 2004; Zanetti et al., 2016).

Late stages of porous-flow melt migrations crystallised apatite- and dolomite-bearing wehrlites and apatite-rich, orthopyroxene-bearing peridotites, which sometimes contain carbonate-bearing domains showing marked modal and geochemical gradients with the host rocks (Zanetti et al., 1999; Morishita et al., 2003, 2008; Matsumoto et al., 2005; Raffone et al., 2006). U–Pb analyses on apatite and isotopic noble gas data have yielded Triassic ages (Morishita et al., 2008).

Apatite and calcite also occur in dykes of nepheline-bearing syenites of the Triassic age, associated with hornblendites (Stähle et al., 1990, 2001). An Early Jurassic U–Pb zircon age was determined for an alkali pegmatite (Grieco et al., 2001).

The rocks of the FPP related to the main event and the dunite bodies show similar geochemical features and absence of geochemical gradients. The harzburgite–pyroxenite association and the chromitite and pyroxenite layers in dunite bodies are depleted in Nb and high field strength elements and significantly enriched in K, Rb, Ba, Sr, and light rare earth elements (LREEs) (Hartmann & Wedephol, 1993; Zanetti et al., 1999, 2016; Mazzucchelli et al., 2014). The mineralogical and compositional features have been considered by several authors as evidence of the role of a slab-derived crustal component in the percolating melts (Hartmann & Wedephol, 1993; Mazzucchelli et al., 1995, 2016; Rivalenti et al., 1995, 2007a; Zanetti et al., 1999, 2016; Grieco et al., 2001, 2004; Morishita et al., 2003, 2008; Ponce et al., 2015; and others). Thus far, a variety of different geochemical components has been identified based on isotopic data. In particular, the Hf (in zircon) and O (in zircon and pyroxene) isotopic compositions of chromitites suggest the presence of large volumes of continental crust in the migrating melts (Zanetti et al., 2016; Malitch et al., 2017), whereas the hydrogen, oxygen, and chlorine isotopic compositions of amphibole and phlogopite from the harzburgite-pyroxenite association show variability (δD from −29 to −86‰, δ^{18}O from 4.9 to 6.1‰, and δ^{37}Cl from −2.0 to +2.1‰) consistent with mixtures of magmatic fluids contaminated by seawater (Hartmann & Wedepohl, 1993; Selverstone & Sharp, 2011).

Giovanardi et al. (2013) reported the occurrence in the FPP of late sapphirine-bearing gabbroic dykes. These dykes crosscut at high angles the pervasive mantle foliation and other lithologies, showing different mineralogical and major element mineral chemistry features with respect to other FPP rocks.

3. Samples and petrography

Two different dykes and their host peridotites from the FPP unit were investigated. The first dike (sample FI09C06, Fig. 2) was collected along the road that connects National Road 631 to a peridotite quarry located on the right flank of the Rio Creves valley (less than 100 m from the outcrops studied by Zanetti et al., 1999). The second dike (sample FI9664) is from a boulder along the Rio Creves, about 30 m upstream of its intersection with the Rio Cannobino. The host peridotite was collected 8 cm from the FI09C06 dyke, and close to the contact with the dyke represented by sample FI9664.

The gabbroic dykes are centimetric in thickness (mostly 2–5 cm; Fig. 2). They show variable strikes, usually crosscutting the harzburgite-pyroxenite association at high angles (Fig. 2).

A Mesozoic age for these sapphirine-bearing dykes is constrained by the observation that they also crosscut the foliation of protomylonites in the external domains of Mesozoic shear zones (Matysiak & Trepmann, 2015 and references therein), but are themselves deformed in a few cm-wide mylonitic to ultramylonitic bands parallel to the protomylonite foliation (Tommasi et al., 2017). Such shear zones were active at different crustal levels over a very long, Triassic–Jurassic time interval (235–180 Ma; Langone et al., 2018 and references therein). This finding is also consistent with the observation that all the late intrusive bodies, which are discordantly intruding the pervasive mantle foliation by hydraulic fracturing, do not show ages older than Triassic (Stähle et al., 1990, 2001; Grieco et al., 2001; Matsumoto et al., 2005).

The gabbroic dykes contain sapphirine (Giovanardi et al., 2013) and show a banded symmetric structure consisting of melanocratic zones at the peridotite contacts and a leucocratic zone representing the dyke core (Fig. 2). The melanocratic zones, in turn, can be divided in three different bands.

From the host peridotite to the dyke core, the following layers can be recognised:

1) An orthopyroxenite zone (hereafter, the Orthopyroxene Zone), established within the ambient peridotite. Orthopyroxene locally shows recrystallised rims with the growth of fine neoblasts of orthopyroxene and rarely olivine. The orthopyroxene sometimes presents exsolution lamellae. Locally, black spinel and phlogopite occur as accessory phases. Phlogopite is concentrated in interstitial positions but rarely fills fractures within orthopyroxene crystals (Fig. 2). Giovanardi et al. (2013) reported the occurrence of a sapphirine- and amphibole-bearing recrystallisation front in the Orthopyroxene Zone.

2) A first melanocratic zone (hereafter, the Early Amphibole Zone) inside veins formed by dark-brown amphibole (up to 1 cm long, named 'early amphibole') and associated small plagioclase grains, spinel, phlogopite, and apatite; in these zones, the magmatic texture is preserved, as evidenced by amphibole twinning. Apatite and spinel mainly occur as rounded inclusions in amphibole, whereas phlogopite is in interstitial position.

3) A second melanocratic zone (hereafter the Late Amphibole Zone), consisting of light-brown to green amphibole (named 'late amphibole'), green spinel, sapphirine, and phlogopite. Sapphirine occurs in three textural positions: inclusions within late amphibole, coronas rimming spinel, and

isolated/aggregated crystals in interstitial positions (Fig. 2). Phlogopite is an accessory phase in interstitial positions. Late amphibole is smaller than early amphibole and is euhedral to anhedral in shape. Intermediate green–brown amphibole, often associated with spinel and sapphirine, is recognised near and through the Early Amphibole Zone–Late Amphibole Zone contact. Recrystallisation zones with a fine-grained texture occur. The Late Amphibole Zone is not continuous through the dykes. It forms patches, which can also occur only on one side of the leucocratic core of the dyke, or that can extend up to the Orthopyroxene Zone. The Late Amphibole Zone is more developed in sample FI9664 (up to about 1.5 cm in thickness) than in sample FI09C06 (up to 1 cm in thickness). In addition, sapphirine crystals in sample FI9664 can reach up to 1.5 mm in size, whereas in sample FI09C06, they are commonly < 0.2 mm.

4) A leucocratic zone (Leucocratic Zone, hereafter) formed by plagioclase and subordinate amphibole (both magmatic and relict from melanocratic zones). Apatite occurs as an accessory phase, sometimes included in plagioclase or in relicts of brown early amphibole. The apatite rarely contains calcite inclusions. Plagioclase shows twinning (mainly pericline and subordinately crossed albite and pericline), which is often partially or totally erased by recrystallisation induced by late deformation. Magmatic amphibole has greenish pleochroism, whereas relict amphibole, ripped from the melanocratic zones, is brown. Amphibole often forms single-crystal alignments parallel to the dyke strike, like in a flow texture. Phlogopite is rare and is associated with amphibole. Recrystallisation zones show fine-grained equigranular texture. Rarely, Fe-oxides, Fe–Ni sulphides, and pyrite occur.

The host peridotite away from the contact is a hornblende-harzburgite in modal composition with a porphyroclastic texture (Giovanardi et al., 2018). It is characterised by the presence of olivine and orthopyroxene porphyroclasts, with a secondary, undeformed mineral assemblage dominated by amphibole (15% by volume), in association with orthopyroxene, spinel, phlogopite, and clinopyroxene, strictly similar to the dominant peridotite type described by Zanetti et al. (1999) and Tommasi et al. (2017). A detailed petrographic inspection highlights the occurrence of a reacted peridotite zone approaching the orthopyroxene zone. It is characterised by the presence of a secondary mineral assemblage, modally dominated by long (up to 5 mm) phlogopite lamellae, with associated subordinate amounts of undeformed orthopyroxene, spinel, amphibole, and clinopyroxene. In the reacted zone, olivine was stable; conversely, the modal orthopyroxene content is slightly lower than that in the peridotite far from the vein. Primary (e.g. olivine) and secondary minerals in the reacted zones display elongation sub-parallel to the present-day vein strike.

4. Analytical methods

Sample FI9664, representing the gabbroic dyke and the contact host harzburgite, was analysed for whole-rock major and trace elements. Whole-rock major elements and Sc, V, Cr, Co, Ni, Cu, and Zn were analysed by X-ray fluorescence spectrometry (XRF), whereas Li, Rb, Sr, Y, Zr, Nb, Ba, rare earth element (REE), Hf, Ta, and Pb contents were analysed by inductively coupled plasma-mass spectrometry (ICP-MS). Analyses were performed following the methods described by Mazzucchelli et al. (2010) (data reported in Supplementary Material A).

Samples FI9664 and FI09C06 were analysed for mineral major elements with the electron microprobe JEOL 8200 Super Probe housed at the University of Milano. Analyses were performed following methods described by Ponce et al. (2015). Data are reported in Supplementary Material A.

Mineral trace elemental contents were determined (as in Rivalenti et al., 2007b) with a LA-ICP-MS housed at Istituto di Geoscienze e Georisorse, Consiglio Nazionale delle Ricerche, Sede Secondaria di Pavia (data are reported in Supplementary Material A) using a Perkin Elmer SCIEX DCR-e coupled with a solid-state laser source (Q-switched Nd:YAG, Quantel Brilliant). Data reduction was performed using the GLITTER software (Griffin et al., 2008). NIST SRM 610 was used as an external standard. Ca was used as an internal standard for clinopyroxene, amphibole, and plagioclase, Si for olivine, orthopyroxene, and phlogopite, and Mg for spinel. Precision and accuracy were assessed by repeated analysis of the standard BCR-2g and were found to be better than 10% at the ppm concentration level. Further information is reported by Giovanardi et al. (2017).

Sample FI09C06 was selected for O, Nd, and Sr isotopic analyses in mineral separates, after the combination of preliminary electron microprobe and LA-ICP-MS analyses suggested a more primitive nature for its parental melt.

O isotopes of pure mineral separates from sample FI09C06 were analysed at the I.G.G.-C.N.R., Pisa, by conventional laser fluorination with a Finnigan Delta Plus mass spectrometer. For each phase, 1–1.5 mg aliquots were necessary to measure the oxygen isotope composition. Analyses were performed following the methods described by Perinelli et al. (2011). Data are reported in Table 1.

Sr and Nd isotopic ratios of amphibole and plagioclase separates from sample FI09C06 and the host harzburgite were analysed at the Marine Environmental Sciences Laboratory (LEMAR) of the Institut Universitaire Européen de la Mer (IUEM), Université de Bretagne Occidentale. Analyses were carried out after dissolution and chromatographic separation using a TRITON Thermo-Ionisation Mass Spectrometer (TIMS), following the procedure described by Janin et al. (2012). Analyses were corrected for the reference material NBS987 ($^{87}Sr/^{86}Sr = 0.710241 \pm 0.000019$, n = 6) for Sr and the La Jolla standard ($^{143}Nd/^{144}Nd = 0.511847 \pm 0.000009$, n = 3) for Nd. Data are reported in Table 2.

5. Bulk rock chemistry

The gabbroic dyke FI9664 presents higher TiO_2, Al_2O_3, CaO, Na_2O, and K_2O contents and lower FeO and MgO contents than the host harzburgite collected at the contact.

The gabbroic dyke has trace element abundances that are one order of magnitude higher than those of the host harzburgite; only Rb and Li contents are similar in both rocks (Fig. 3; Supplementary Material A). The two rock types show some similarities in element fractionation: marked enrichments in LREEs with respect to middle-heavy rare earth elements (M-HREE; $(La/Yb)_N$

values are 5.5 and 16–30 for the dyke and host harzburgite, respectively; primitive mantle data from McDonough and Sun, 1995); $(Th/U)_N$ and $(Zr/Hf)_N$ always < 1; and positive Ba and Pb anomalies. Conversely, the $(Nb/Ta)_N$ values are 1.6 for the gabbroic dyke and 0.7 for the host harzburgite.

Linearly fractionated LREE-enriched patterns were also shown by the nepheline-bearing alkaline dykes described by Stähle et al. (2001). However, the latter had significantly higher trace element contents than those of gabbroic dyke FI9664. The dykes reported by Stähle et al. (2001) also displayed significant peculiarities in terms of fractionation of highly incompatible trace elements, such as U, Th, Nb, Ta, Ba, and Pb, with respect to REEs.

The spidergram of the peridotite close to the contact with dike FI9664 shows some relevant differences with respect to those reported by Hartmann & Wedephol (1993): large positive Pb and Hf anomalies, greater Rb, U, Ba, Ta, and Nb contents, and slightly lower LREE contents (Fig. 3).

6. Major element mineral chemistry

6.1. Host harzburgites

The mineral composition of the host harzburgite far from the veins is similar to that of the harzburgite-pyroxenite association reported by Zanetti et al. (1999). The amphibole is pargasitic in composition, with only one analysis of Mg-hornblende composition. The mica is phlogopite, and the clinopyroxene is diopside.

Minor differences include a slightly Fe-enriched composition shown by olivine (Fo = $100 \times Mg/(Mg + Fe^{2+}_{tot})$, molar ratio of 90.4–91.1), orthopyroxene, spinel, and amphibole (Fig. 4). Orthopyroxene and spinel (hercynite to spinel in composition) are also richer in Al. Because of their low Cr#, the FI09C06 oxides straddle the hercynite–spinel boundary, whereas oxides in the FPP are chromite. Lower Cr content is shown by amphibole, which is also characterised by lower Na and higher K contents.

At the contact with the vein, the Mg# does not change significantly in the minerals. Aluminium decreases in orthopyroxene, spinel, amphibole, and phlogopite, whereas Ti content is higher in both amphibole and phlogopite. In amphibole, Na decreases, balanced by higher K content (Fig. 5). Conversely, the Na/K ratio is very variable in phlogopite.

Orthopyroxene from the Orthopyroxene Zone has lower Mg# and CaO content and higher Al_2O_3 content (Fig. 4). Similarly, its composition is different from orthopyroxene from the sapphirine-bearing rock found in the LIZ northern unit of the Finero Mafic Complex by Sills et al. (1983). The latter has lower Mg# and higher Al_2O_3 content (Fig. 4).

6.2. Gabbroic dykes

Notwithstanding the similar internal banding, the two studied dykes show marked differences in terms of major elemental mineral chemistry. Significant compositional changes are also shown for the different types of amphibole (i.e. the Early and Late Amphibole Zones and the Leucocratic Zone; Fig. 6). The unique common feature of the amphiboles of both gabbroic dykes is the higher Al content exhibited by the late amphibole (Giovanardi et al., 2013). Amphibole from gabbroic dykes is mostly pargasitic in composition (unit formula calculated according to Ridolfi et al., 2018), but sometimes Al substitution for Si in late amphibole is higher than 2 a.p.f.u., thereby entering the sadaganaite compositional field.

In particular, amphibole from sample FI09C06 has distinctly lower Mg# (0.73–0.82) than sample FI9664 (0.85–0.87). In sample FI09C06, Mg# is lower in early amphibole than in late and leucocratic amphibole, whereas it is exactly the reverse in sample FI9664 (Fig. 6).

FI09C06 amphibole also displays the lowest CaO and Na_2O and the highest TiO_2 and K_2O contents (TiO_2 0.27–2.19 wt.% and K_2O 0.31–1.28 wt.% respectively) (Fig. 6).

In sample FI09C06, TiO_2 linearly increases with the decrease in Mg#. Instead, TiO_2 is higher in the FI9664 early amphibole than in the leucocratic amphibole, but distinctly higher TiO_2 contents are shown by late amphibole. Moreover, in sample FI9664 early amphibole, the increase in Mg# is associated with increasing Cr and Ca, and with decrease in Na and Al contents.

As a whole, amphibole from the gabbroic dykes has higher Al_2O_3 content and lower Mg# and Cr_2O_3 content with respect to others FPP lithologies, resulting in similarity to the amphibole from the sapphirine-bearing rock in the LIZ (Sills et al., 1983) (Fig. 6). Amphibole from the two gabbroic-dykes samples shows lower CaO and K_2O and higher Na_2O contents than the respective host amphibole (Fig. 6).

Phlogopite from sample FI9664 presents a narrow range of major elemental contents with respect to sample FI09C06. In sample FI9664, phlogopite has higher Mg# values than phlogopite from sample FI09C06 (0.92–0.94 and 0.70–0.90, respectively) and commonly lower TiO_2 contents (Fig. 5). Phlogopite from the gabbroic dykes shows higher Al_2O_3 content and lower Mg# than the phlogopite from the host peridotite and the harzburgite-pyroxenite association (Fig. 5).

Spinel is mainly found in the Late Amphibole Zone. Unlike the spinel from the host harzburgite, the harzburgite-pyroxenite association reported by Zanetti et al. (1999), and the chromitite layers in dunite bodies (Grieco et al., 2001; 2004; Zanetti et al., 2016), the spinel from the gabbroic dykes does not contain Cr_2O_3 and can be classified as spinel (Mg# 0.46–0.75).

Plagioclase from sample FI9664 is commonly more anorthitic than the plagioclase from sample FI09C06 (An contents of 82–93 and 36–87, respectively). In both samples, some reversely zoned plagioclases are recognised.

The sapphirine composition falls near the 7:9:3 composition on the SiO_2–(FeO + MgO)–(Al_2O_3 + Cr_2O_3 + Fe_2O_3) diagram (Fig. 7). Sapphirine from sample FI9664 is higher in Al_2O_3 content with respect to sample FI09C06, whereas it is lower in SiO_2 content.

Scanning electron microscope (SEM) investigations at the Centro Interdipartimentale Grandi Strumenti laboratories of the Università di Modena e Reggio Emilia, performed with an Environmental SEM Quanta-200 (Fei Company-Oxford Instruments), suggest that apatites from different zones of the dykes are Cl-apatites.

7. Trace elemental compositions

7.1. Host harzburgite

Amphibole and clinopyroxene from harzburgite FI09C06, 8 cm away from the contact with the gabbroic dyke, are characterised by LREE-enriched linearly fractionated patterns (Figs. 8, 9 and 10). Their compositions are similar to those of the FPP harzburgite-pyroxenite association (Zanetti et al., 1999). Proceeding toward the contact (i.e. sample FI9664), amphibole and clinopyroxene show upward-convex REE patterns characterised by high variability in absolute contents (Figs. 8, 9 and 10). These patterns are similar to those from apatite-rich domains reported by Zanetti et al. (1999) (Figs. 9 and 10).

7.2. Gabbroic dykes

The two gabbroic dykes show different trace element compositions. In sample FI09C06, amphiboles from the Early Amphibole Zone and Leucocratic Zone have L-MREE-enriched upward-convex patterns, similar to those of harzburgite near the contact (Fig. 8). In the Late Amphibole Zone, some crystals show more fractionated patterns characterised by lower M-HREE contents and positive Eu anomalies (Fig. 8). These variations are associated with marked depletion in Ta, Zr, Hf, Y, Sc and V (Fig. 10, V is not shown). As a whole, amphiboles from different zones of sample FI9664 show more fractionated REE patterns characterised by enrichment in LREEs and depletion in HREEs (Fig. 8) with a nearly flat pattern in the LREE region. Amphibole from the Early Amphibole Zone of sample FI9664 presents a small positive Eu anomaly ($(Eu/Eu^*)_N$ within 1.04–1.65), which becomes more evident in the amphibole from the Late Amphibole Zone ($(Eu/Eu^*)_N$ within 1.29–1.62). Amphibole from sample FI9664 is also more enriched in Th, U, and Pb (and to lesser extent in Sr) compared with amphibole from sample FI09C06 (Fig. 10).

Similar to the amphibole, REE patterns of plagioclase from sample FI9664 are more fractionated than those of plagioclase from sample FI09C06, (Fig. 8). In both samples, the trace elemental abundances of the plagioclase cores are greater than those of the plagioclase rims.

Apatite displays the typical LREE enrichment and high Th, U and Pb contents (12.31–17.35 ppm, 4.35–5.92 ppm, and 2.18–4.19 ppm, respectively). Nb, Ta, Zr, Hf, Ti, and Sc show negative anomalies with values that are often below the detection limit.

No systematic trace elemental variations were found in phlogopite.

8. O isotopes

The $\delta^{18}O$ in silicates of sample FI09C06 shows a steady increase from the contact (Orthopyroxene Zone) to the leucocratic gabbro in the vein core, through the Early and Late Amphibole Zones (Fig. 8, 10, and 11 and Table 1). In particular, it varies from 5.81‰ (standard deviation (std. dev.) 0.11) in orthopyroxene from the Orthopyroxene Zone to 6.9‰ (std. dev. 0.05) in amphibole from the Early and Late Amphibole Zones, and to 8.60‰ (std. dev. 0.01) in the plagioclase of the gabbroic core.

The $\delta^{18}O$ values of orthopyroxene from the Orthopyroxene Zone lie within the mantle range. They are higher than the $\delta^{18}O$ value reported by Hartmann & Wedephol (1993) for clinopyroxene from the phlogopite-bearing amphibole harzburgite (Fig. 11), and for orthopyroxene from olivine-chromitites of the FPP, but significantly lower than the orthopyroxene from orthopyroxene-chromitites (Zanetti et al., 2016).

Vein amphibole and plagioclase have $\delta^{18}O$ values significantly higher than the mantle range (Fig. 11). They are close to the highest values found in amphibole, phlogopite, orthopyroxene, clinopyroxene, and zircon from the phlogopite-bearing amphibole harzburgite-pyroxenites (Hartmann & Wedephol, 1993; Selverstone and Sharp, 2011) and chromitite layers of the FPP (Zanetti et al., 2016).

The $\delta^{18}O$ values obtained for the green spinel associated with sapphirine are markedly lower than those of the associated late amphibole ($\delta^{18}O$ = 4.38‰, std. dev. 0.10), as expected based on crystal-chemical constraints (see Bindeman, 2008 and references therein).

9. Sr and Nd isotopes

The trace elemental concentrations of the mineral separates of early and late amphibole match the differences highlighted by LA-ICP-MS analysis of thin sections. The Sr and Nd isotopic compositions of early amphibole and late amphibole from the FI09C06 dyke are coincident within analytical uncertainty (Table 2). Plagioclase from the FI09C06 Leucocratic Zone shows the same Sr isotopic composition of the amphiboles, and only a slightly more radiogenic ^{143}Nd/^{144}Nd ratio. Similar Sr isotopic compositions were documented in amphibole and apatite of discordant veins from the FPP, which were characterised by higher ^{143}Nd/^{144}Nd ratios (Morishita et al., 2008). The isotopic composition of the dyke minerals is enriched with respect to the depleted mantle reference value and the mid-oceanic ridge basalt (MORB) field; these minerals fall within the ocean island basalt (OIB) field (Fig. 12). In particular, they lie between the isotopic compositions of FPP hornblende-syenite dykes (bulk rock from Stähle et al., 1990, 2001) and peridotites (amphibole and clinopyroxene from Obermiller, 1994). Amphiboles separated from the host harzburgite (collected far from the contact) show the most radiogenic Sr and unradiogenic Nd values, but have never before been documented in the literature for FPP rocks (Fig. 12).

10. Discussion

10.1. Petrogenesis of the sapphirine-bearing gabbroic dykes

The two veins studied here share exactly the same internal banding as the sample described by Giovanardi et al. (2013). This suggests that all three veins were part of an interconnected swarm, which allowed them to record the same sequence of petrologic events. The symmetric structure of the dykes suggests that the intrusion occurred through several events of melt percolation. In the following section, we discuss, in detail, the different stages and processes that produced the gabbroic dyke swarm.

10.1.1. Melt percolation though the peridotite

According to the process governing the emplacement of other dyke swarms in mantle sectors (e.g. Mazzucchelli et al., 2010 and references therein), the melts flowing in the metasomatic haloes and in the conduit were originally similar, undergoing severe fractionation owing to assimilation and fractional crystallisation.

The characterisation of the wall peridotite has revealed some peculiarities. It is a common observation that metasomatic haloes of cm-to-m-scale surround late dykes and veins formed by melt segregation under mantle conditions. In most cases, the metasomatic haloes show marked geochemical and mineralogical gradients as a function of the distance from the dike contact (Zanetti et al., 1999; Ionov et al., 2002, Mazzucchelli et al., 2010; Borghini et al., 2016, 2017), which are interpreted as the result of porous flow percolation of melt escaping from the open conduits. Conversely, no progressive mineralogical or compositional variation is documented in the wall peridotite of sample FI9664 at a variable distance from the vein (see Supplementary Material B). Newly-formed clinopyroxene actually shows trace element heterogeneities, but these are randomly distributed. Conversely, the trace element composition of amphibole is very homogeneous, indicating late crystallisation from a unique melt.

The particular L/MREE-enriched convex-upward patterns shown by clinopyroxene and amphibole from the wall peridotite of sample FI9664 also demonstrate that their parental melt could not have been the same as that from which the adjacent early amphibole of dyke FI9664 crystallised (which show linearly-fractionated REE patterns). However, based on the amphibole trace element composition, the melt recorded by the wall peridotite of sample FI9664 must have been quite similar to the melt that produced the Early Amphibole Zone of dyke FI09C06.

The textural evidence that primary and secondary minerals from the metasomatic haloes display elongation sub-parallel to the present-day vein strike confirms that the development of melt migration channels was associated with some local deformation.

These observations can be reconciled by assuming that the metasomatic haloes were not produced by melt escaping normally from the conduit. They were likely established during an early stage of melt migration via focused porous flow along channels developed in correspondence with structural weakness, with a direction roughly parallel to the strike of the present-day veins.

The absence of resorption textures in olivine of the reacted wall peridotite indicates that this mineral was stable. Conversely, the modal content of orthopyroxene is slightly lower than in the peridotite far from the vein. This evidence leads us to consider that the orthopyroxene saturation of the melts, indicated by the segregation of the reactive Orthopyroxene Zone and the presence of few orthopyroxenes in the veins (Giovanardi et al., 2013), was not a clear, primary characteristic, but possibly a consequence of an early stage of reactive melt migration characterised by olivine precipitation and orthopyroxene dissolution (see Piccardo et al., 2017).

The mineralogical mismatch between the nearly monomineralic, hydrous-mineral-free Orthopyroxene Zone and the Early Amphibole Zone suggests that they were segregated by compositionally different melts. This hypothesis is confirmed by large differences in terms of O isotopic compositions recorded by the orthopyroxene (5.8‰ standard mean ocean water (SMOW)) from the Orthopyroxene Zone and the amphibole from the Early Amphibole Zone (6.9‰ SMOW) within the vein. The lighter O isotopic composition of the Orthopyroxene Zone would support a hybrid composition of its parental melt caused by reactive porous flow through the FPP, with buffering of O isotopic composition at mantle values.

This conclusion led us to consider the possibility that the Orthopyroxene Zone formed before the segregation of the Amphibole Zones, possibly at the centre of the migration channels, as observed elsewhere in the FPP. It was successively split into two parts by the opening of the fracture.

10.1.2. Melt segregation in the open conduit

The Early Amphibole Zone was segregated when melts started flowing in open fractures. It is likely that amphibole crystallisation was triggered by the presence of an ultramafic wall, suggesting that plagioclase was unstable in contact with the orthopyroxenite layers. The development of amphibole-rich selvages where hydrous gabbroic rocks come in contact with ultramafic layers (e.g. in the LIZ of the Finero Complex; Mazzucchelli et al., 2014) has previously been documented in the literature.

The two gabbroic dykes of this study show significant differences in terms of major and trace element mineral compositions. In particular, amphibole from the FI9664 vein shows an unusual relative enrichment in highly incompatible trace elements (U, Th, LREEs, and Na) and compatible elements (Mg, Ca, and Cr) with respect to those from the FI09C06 vein. Consistently, phlogopite is more enriched in Mg and Na, and plagioclase is more anorthitic. Assuming that the dyke swarm was produced by the injection of a unique melt, this relationship cannot be reconciled based on a melt evolution governed only by fractional crystallisation. Mazzucchelli et al. (2010) documented the same correlation between compatible and incompatible elements in minerals from cm-thick diorite dykes, demonstrating that such geochemical features can be modelled considering an assimilation of host minerals concomitant with fractional crystallisation (i.e. assimilation and fractional crystallisation (AFC) processes). Accordingly, we argue that the parental melt of vein minerals in sample FI9664 can be considered more evolved through AFC processes than that of dyke FI09C06. The concomitant enrichment of Na and Ca in the vein minerals of sample FI9664 evidences the role of amphibole in the assimilated component. This is also confirmed by the trace element patterns of FI9664 vein amphiboles, in which highly incompatible elements (such as LREEs, Th, and U) increase and moderately incompatible element (such as HREEs, Ti, and Y) decrease, moving toward the fractionation shown by those of host harzburgite away from the contact. The decrease of moderately incompatible elements with the progression of the melt evolution may be indicative of ${}^{\mathrm{Amphibole/L}}D$ higher than 1 (Tiepolo et al., 2007). It is noteworthy that the Al content in sample FI9664 early amphibole is comparable with to slightly lower than in those from the FI09C06 vein, suggesting that the assimilation of host minerals was not effective in boosting the Al concentration of the evolving melt.

10.1.3. Formation of sapphirine-bearing patches

The mm-to-cm-thick sapphirine-bearing patches and stripes are randomly distributed from the internal end of the hornblendite seam to the Orthopyroxene Zone, although they are generally concentrated towards the centres of the veins. They are apparently the results of interstitial migration of a melt in chemical disequilibrium with the early cumulus minerals, as indicated by the recrystallisation fronts inside large early amphiboles. Both interstitial and recrystallised patches show that the injected melt was saturated in late amphibole, sapphirine, and spinel, whereas the saturation in phlogopite is uncertain, because it occurs only interstitially and the textural relationships are equivocal.

The following series of petrographic and geochemical features suggest that the sapphirine-bearing mineral assemblages were not simply related to interaction with the parental melt of the Leucocratic Zone, but were segregated because of the injection in the dyke swarm of an additional melt component coming from outside the system:

1) Early amphibole at the contact with or embedded by the plagioclase of the Leucocratic Zone does not show any evidence of comparable reaction.
2) Notwithstanding the significantly different major elemental composition of early amphibole documented in the two veins of this study, the major elemental chemistry of sapphirine-associated late amphibole converges toward specific Al and Mg# values. Phlogopite shows consistent variation, even though its attribution to early or late amphibole assemblages is doubtful because of its interstitial position. The data reported by Giovanardi et al. (2013) confirm this trend. This finding indicates that a unique component with a specific composition was responsible for the sapphirine segregation in the three sectors of the dyke swarm.
3) Normalised patterns of late amphibole from sapphirine-bearing areas show particular features: stronger LREE/HREE fractionation, depletion in M-HREEs, Zr, Hf, Nb, Ta, Ti, Sc,

and V, and the appearance of a positive Eu anomaly. The results also show inversion of the $(Zr/Hf)_N$ values, which are > 1 in the early amphibole, but < 1 in the late amphibole. The overall fractionation mimics that normally exhibited by plagioclase.

The latter evidence, consistent with the apparent increase of the Al content in the system, suggests that the injected melt was characterised by a high normative plagioclase content.

The O, Nd, and Sr isotopic compositions of early and late Amphibole are very similar, suggesting that the plagioclase component belonged to the same magmatic cycle that produced the dyke swarm.

However, petrographic surveying has not provided evidence of plagioclase assimilation and/or replacement by amphibole or another mineral, excluding plagioclase components derived by local assimilation. Thus, we suggest that the plagioclase signature was acquired by the injected melt through assimilation of cumulus plagioclase in hidden magmatic bodies and/or addition in the melt source, where it was likely present as a high-P metamorphic equivalent of pristine plagioclase.

10.1.4. Segregation of the Leucocratic Zone

The petrographic evidence confirms that the formation of the Leucocratic Zone was a high energy event, which determined the partial disaggregation of the Early Amphibole Zone, with evident breaking of large early amphibole crystals. It can be locally recognised that two parts of a formerly unique crystal apparently lie on different sides of a vein. Giovanardi et al. (2013) suggested that this stage was accompanied by enlargement of the conduits.

The Nd and Sr isotopic compositions of the plagioclase indicate that the parental melt had a cognate origin with those of the hornblendite selvages. This inference is also confirmed by the trace element composition of the leucocratic amphibole, which is strictly similar to that of the associated early amphibole.

Nevertheless, the observation that the major elemental chemistry of the leucocratic amphibole is intermediate between that of early and late amphibole leads us to conclude that the parental melt of the sapphirine-bearing assemblages could be still present in diluted proportions.

10.2. Nature of the parental melts

Evaluating the nature of the parental melt of magmatic segregates belonging to narrow, cm-thick veins/dykes intruding mantle peridotites at high-T-P mantle conditions must be done with particular caution, with an effort first to characterise the modifications imparted by fractional crystallisation and the reaction/assimilation processes with the host rock (e.g. Mazzucchelli et al., 2010 and references therein). As discussed in the previous section, sample FI09C06 shows that its parental melt underwent the lowest degree of interaction with the host peridotite among the known dykes, and thus is the best candidate to obtain constraints on the nature of the parental melts.

An important contribution in defining the geochemical components in the melts is provided by the marked zoning in terms of O isotopic composition documented in sample FI09C06 between the Orthopyroxene Zone, the hornblendite selvage, and the Leucocratic Zone.

The δ^{18}O values of early and late amphibole (6.9‰ SMOW) well exceed the mantle range (Bindeman, 2008; Polat et al., 2018), suggesting a large contribution by crustal components in the parental melt of sample FI09C06 hornblendite. The proportion of the crustal component is even larger in the leucocratic band, in which a δ^{18}O value of 7.8‰ SMOW can be calculated for the amphibole in hypothetical equilibrium with the plagioclase composition (8.6‰ SMOW). This is done by conservatively considering a low closure T for the FPP of ~850 °C (provided by pyroxene-solvus geothermometry), an average value of An70 for plagioclase, and the δ^{18}O mineral fractionation values reported by Bindeman (2008).

Published data on FPP minerals show a pronounced heterogeneity of the O isotopic composition, with δ^{18}O values from below to well above the mantle range (Hartmann and Wedephol, 1993;

Selverstone and Sharp, 2011; Zanetti et al., 2016). This heterogeneity may be due to multiple melt-migration events.

Values of $\delta^{18}O$ approaching those of early and late amphibole have sometimes been documented in harzburgites and chromitites (Hartmann & Wedephol, 1993; Zanetti et al., 2016), but the values of the leucocratic layers are markedly out of range.

In addition, the $\delta^{18}O$ value shown by orthopyroxene (5.81‰ SMOW) from the Orthopyroxene Zone provides a very important constraint, indicating how migrating melts, after prolonged interaction with the FPP, may have oxygen isotopic compositions buffered to mantle values. The decrease of $\delta^{18}O$ values in the minerals from the hornblendite selvages with respect to those from the dyke core (i.e. the Leucocratic Zone) confirms such a buffering effect.

We conclude that the high $\delta^{18}O$ shown by dyke minerals cannot be the result of interaction between melts and the FPP but is a primary feature of the melts, which indicates the occurrence of large amounts of crustal components, either added to the melt in the source regions or at greater mantle depths.

A subduction-related component was identified based on noble gas isotopic composition in Late Triassic apatite-rich layers (Matsumoto et al., 2005, Morishita et al., 2003, 2008), overprinting the crustal affinity of the host FPP. Amphiboles from such apatite layers show the same radiogenic Sr isotopic composition as the minerals of sample FI09C06, coupled to a slighter more radiogenic Nd isotopic composition.

The isotopic compositions of early amphibole, late amphibole, and plagioclase from the FI09C06 dyke are significantly richer in radiogenic Sr and unradiogenic Nd isotopes compared with those reported from nepheline-bearing Triassic intrusions cutting the FPP (Stähle et al., 1990, 2001), which were interpreted as derived from alkaline melts of OIB affinity.

Combining data from nepheline-bearing alkaline dykes, sapphirine-bearing dykes, and the FPP, we can define a trend at low radiogenic Nd and high radiogenic Sr isotopic ratios, suggesting mixing between asthenospheric components (OIB, according to Stähle et al., 1990; 2001 and Schaltegger et al., 2015) with materials derived from the continental crust (see compositional fields of Casetta et al., 2018a). We speculate that the crustal components were located at lithospheric deep levels after the Variscan orogenic cycle (e.g. Bonadiman et al., 1994) and mobilised by asthenospheric magmatism. This scenario is supported by the evidence of continental crustal metasomatism exhibited by mantle bodies involved in the Variscan collisional orogeny, such as the FPP, the Ulten Zone (Sapienza et al., 2009), and some of the Bohemian Massif (Becker et al., 1999; Schulmann et al., 2014).

In this scenario, it can be noted that the Nd and Sr isotopic compositions of sample FI09C06 lie on the mixing line between the composition of the Triassic alkaline dykes and the host harzburgite away from the contact. According to AFC simulation, assimilation of significant degrees of the metasomatised peridotite material (15%) into OIB must be considered to account for the composition of the parental melt of the FI09C06 veins.

Comparison of the trace elemental patterns of the amphibole from the vein apparently less contaminated by the host peridotite (FI09C06) with those of amphiboles segregated by primary hydrous alkaline basalts (e.g. Demeny et al., 2005) shows similarity in REE fractionation, but the early amphibole has an absolute content that is nearly one order of magnitude higher. In addition, a correlation with primary alkaline mantle melts is not directly supported by the negative Nb, Ta, and Ti anomalies shown by the early amphibole.

Equilibrium liquids calculated from the trace elemental composition of early amphibole from the FI09C06 dyke and amphibole-melt partition coefficients experimentally determined at 1,015 °C in the presence of moderately polymerised melts (dataset T2 1015; Tiepolo et al., 2007) match the REE contents and fractionation exhibited by shoshonitic rocks of the Triassic magmatism of the Dolomites area (Casetta et al., 2018a; 2018b; see Supplementary Material C). The calculated melts also show consistent negative Ti anomalies, $(Nb/La)_N$ values close to 1, and slight positive U, Th, and Pb anomalies; the latter are more pronounced in the shoshonitic melts. However, a best match in terms of U, Th, and Pb concentrations is shown by equilibrium liquids calculated in equilibrium with amphiboles from 9,664 dykes. These observations suggest that the sapphirine-bearing gabbroic dykes may record the deep mantle input of Triassic K-rich calc-alkaline to shoshonitic melts erupted into the eastern Southern Alps, also documenting the fractionation trends responsible for the enrichment in Th, U, and Pb. This hypothesis is also supported by the Sr and Nd isotopic compositions of Triassic K-rich calc-alkaline to shoshonitic intrusive rocks and lavas of the Eastern Alps (Casetta et al., 2018a; Figure 12), which approach the isotopic trend defined by our model.

10.3. Constraints on the geodynamic evolution of the Europe–Africa boundary

10.3.1. P–T constraints on the FPP

Geothermobarometric estimates constrain the intrusion of sapphirine-bearing dykes at very high-P and T conditions. Ab-initio calculations indicate that the primary crystallisation field of sapphirine in the MAS diagram (SiO_2–MgO–Al_2O_3) becomes considerably larger over 1.0 GPa and shrinks at 2.0 GPa (Belmonte et al., 2014). This evidence confirms the experimental results of Liu & Presnall (1990, 2000) and Milholland & Presnall (1998), indicating that magmatic sapphirine in FPP veins likely crystallised at P ≥ 1 GPa. Equilibrium T estimates based on the sapphirine–spinel Mg–Fe^{2+} exchange thermometer of Sato et al. (2006) and the amphibole–plagioclase thermometer of Holland & Blundy (1994) are mostly higher than 1,000 °C (up to 1,085 °C), confirming the T estimates of Giovanardi et al. (2013). The melt T was thus significantly higher than that in the host harzburgite, which shows solidus T typically corresponding to the water-oversaturated peridotite (965 °C at P = 1.1 GPa; Giovanardi et al., 2013). The absence of partial melting evidence in the host FPP confirms that the source of the uprising melts was at greater mantle depths. The high T, in combination with the high water and volatile contents, may have allowed the melt to migrate via porous flow along the direction of structural weakness (see Tommasi et al., 2017) before the opening of the conduits.

The high-P emplacement conditions are consistent with the scenario where the FPP, after Palaeozoic metasomatism, remained at depths greater than the large lherzolitic mantle bodies south of the Anzola-Val Grande high-T shear zone (namely, from north to south, Premosello, Balmuccia, and Baldissero; Quick et al., 1995), until its exhumation at shallower levels at ~180 Ma (Zanetti et al., 2013, 2016; Langone et al., 2017, 2018; Decarlis et al., 2017, Malitch et al., 2017; Petri et al., 2019).

10.3.2. Constraints on the Mesozoic mantle sources at the Africa–Europe Boundary

The outcomes of this study indicate that in the Mesozoic, melts extremely rich in volatiles (H_2O, P, CO_2, and Cl), K, Na, and highly incompatible elements rose from mantle depths toward the surface. The large crustal component present in the melts, as indicated by the O isotopic composition, leads us to consider that the high Al content, enrichment in large-ion lithophile elements and LREEs, and enriched Nd and Sr isotopic compositions are a primary feature inherited from the source.

This finding confirms the extreme complexity of the tectono-magmatic scenario recorded by the FPP. In particular, the northern IVZ records an extremely prolonged release of K-H_2O-rich mantle-derived melts mixed with subduction-related components, which lasted from the Variscan orogenic cycle to the Mesozoic exhumation of lithospheric mantle at shallower levels. This explains why the FPP records many generations of phlogopite-bearing mineral assemblages, showing variable field relationships, geochemical signatures, and ages (Hartmann & Wedephol, 1993; Zanetti et al., 1999; 2013; 2016; Stähle et al., 1990; 2001; Greco et al., 2001; 2004; Morishita et al., 2003, 2008; Malitch et al., 2017). It also provides a new interpretative frame for previous data indicating the emplacement of melts with subduction-related components in the Triassic (Mastumoto et al., 2005; Morishita et al., 2008, Malitch et al., 2017).

This magmatism-bearing subduction component appears to have roughly overlapped with the ascent of silica-undersaturated alkaline melts of OIB affinity (Stähle et al., 1990, 2001, Schaltegger et al., 2015), which likely also have some counterparts in the central IVZ (Fiorentini et al., 2018; Galli et al., 2019).

The FPP developed in a concomitant extensional–transtensional tectonic regime, the origin and geodynamic scenario of which are still strongly debated (Cassinis et al., 2008; Zanetti et al., 2013; Casetta et al., 2018a, b). Further investigations are needed to address whether the crustal components are remnants of old subduction events (Bonadiman et al., 1994), possibly located at lithospheric levels, reactivated by asthenospheric magmatism with OIB or depleted mantle affinity; represent crustal material recycled into asthenospheric mantle sources (Locmelis et al., 2016); or were added by active Mesozoic subduction (Cassini et al., 2008; Schmid et al., 2008; Morishita et al., 2008; Selverstone and Sharp, 2011; Zanetti et al., 2013).

It is a matter of fact that the major elements (in particular the enrichment in K and Al), trace elements, and Sr and Nd isotopic compositions of the sapphirine-bearing gabbroic rocks approach the geochemical affinity shown by Triassic K-rich calc-alkaline to shoshonitic magmatism of the Dolomites area (Eastern Alps) (Casetta et al., 2018a, b). Thus, the study of magmatic events at the roots of the continental crust of the Adria Plate can provide a unique opportunity to constrain the tectono-magmatic evolution of the Europe–Africa boundary.

11. Concluding remarks

A detailed survey of Mesozoic sapphirine-bearing gabbroic dykes within the FPP unit led us to recognise different stages of melt migration (from porous-flow migration in peridotite channels to flow in open conduits) and constrain the presence in the parental melts of a large continental crustal component acquired in the source region or at deeper lithospheric mantle levels.

The reaction between dyke melts and the strongly metasomatised FPP enhanced the crustal signature.

The high Al content of these melts allowed the segregation of magmatic sapphirine, which is a marker of high-P-T intrusive conditions.

This dyke swarm possibly represents a record of the input to the mantle of the K-rich calk-alkaline to shoshonitic melts that characterised the magmatism widespread during the Triassic in the Southern Alps area.

Acknowledgements

This work was supported by Ministero dell'Istruzione dell'Università e della Ricerca (MIUR), Progetti di Rilevante Interesse Nazionale (PRIN) 2015 Protocol 20158A9CBM. We thank Jean Yves Cottin and Dejan Prelević for their constructive comments and Elsevier Language Editing Services for improving the quality of the text.

References

Becker, H., Wenzel, T., Volker, F., 1999. Geochemistry of glimmerite veins in peridotites from Lower Austria - implications for the origin of K-rich magmas in collision zones. Journal of Petrology 40, 315-338.

Belmonte, D., Ottonello, G., Zuccolini, M.V., 2014. Ab initio thermodynamic and thermophysical properties of sapphirine end-members in the join $Mg_4Al_8Si_2O_{20}$-$Mg_3Al_{10}SiO_{20}$. American Mineralogist 99, 1449-1461.

Bindeman, I., 2008. Oxygen Isotopes in Mantle and Crustal Magmas as Revealed by Single Crystal Analysis. Reviews in Mineralogy & Geochemistry 69, 445-478.

Bonadiman, C., Coltorti, M., Siena, F., 1994. Petrogenesis and T-fO_2 estimates of Mt. Monzoni complex (Central Dolomites,Southern Alps): a Triassic shoshonitic intrusion in a transcurrent geodynamic setting. European Journal of Mineralogy 6, 943-966.

Borghini, G., Rampone, E., Zanetti, A., Class, C., Cipriani, A., Hofmann, A.W., Goldstein, S.L., 2016. Pyroxenite layers in the Northern Apennines' upper mantle (Italy) - generation by pyroxenite melting and melt infiltration. Journal of Petrology 57, 625-653.

Borghini, G., Fumagalli, P., Rampone E., 2017. Partial melting of secondary pyroxenite at 1 and 1.5 GPa, and its role in upwelling heterogeneous mantle. Contributions to Mineralogy and Petrology 172, 70, https://doi.org/10.1007/s00410-017-1387-4.

Casetta, F., Coltorti, M., Ickert, R.B., Bonadiman, C., Giacomoni, P.P., Ntaflos, T., 2018a. Intrusion of shoshonitic magmas at shallow crustal depth: T–P path, H_2O estimates, and AFC modeling of the Middle Triassic Predazzo Intrusive Complex (Southern Alps, Italy). Contributions to Mineralogy and Petrology 173, 57, https://doi.org/10.1007/s00410-018-1483-0.

Casetta, F., Coltorti, M., Marrocchino, E., 2018b. Petrological evolution of the Middle Triassic Predazzo Intrusive Complex, Italian Alps. International Geology Review 60, 977-997.

Cassinis, G., Cortesogno, L., Gaggero, L., Perotti, C. R., Buzzi, L., 2008. Permian to Triassic and magmatic evolution of theBrescian Prealps (eastern Lombardy, Italy). Italian Journal of Geosciences 3, 501-518.

Cawthorn, R.G., 1975. The Amphiboleibole peridotite - metagabbro complex, Finero, northern Italy. Journal of Geology 83, 437-454.

Correia, C.T., Sinigoi, S., Girardi, V.A.V., Mazzucchelli, M., Tassinari, C.C.G., Giovanardi, T., 2012. The growth of large mafic intrusions: Comparing Niquelândia and Ivrea igneous complexes. Lithos 155, 167-182.

Consuma, G., Braga, R., Giovanardi, T., Bersani, D., Konzett, J., Lugli, F., Mazzucchelli; M., Tropper, P. 2019. *In situ* Sr isotope analysis of mantle carbonates: Constraints on the evolution and sources of metasomatic carbon-bearing fluids in a paleo-collisional setting. Lithos https://doi.org/10.1016/j.lithos.2019.105334.

Cumming, G.L., Köppel, V., Ferrario, A., 1987. A lead isotope study of the northeastern Ivrea Zone and the adjoining Ceneri zone (N-Italy): evidence for a contaminated subcontinental mantle. Contribution to Mineralogy and Petrology 97, 19-30.

Decarlis, A., Beltrando, M., Manatschal, G., Ferrando, S., Carosi, R., 2017. Architecture of the distal Piedmont-Ligurian rifted margin in NW Italy: Hints for a flip of the rift system polarity. Tectonics 36, 2388-2406.

Demény, A., Vennemann, T.W., Homonnay, Z., Milton, A., Embey-Isztin, A., Nagy, G., 2005. Origin of amphibole megacrysts in the Pliocene-Pleistocenebasalts of the Carpathian-Pannonian region. Geologica Carpathica 56, 179-189.

Dohmen, R., Blundy, J., 2014. A predictive thermodynamic model for element partitioning between plagioclase and melt as a function of pressure, temperature and composition. American Journal of Science 314, 1319–1372.

Fiorentini, M.L., LaFlamme, C., Denyszyn, S., Mole, D., Maas, R., Locmelis, M., Caruso, S., Bui, T.-H., 2018. Post-collisional alkaline magmatism as gateway for metal and sulfur enrichment of the continental lower crust. Geochimica et Cosmochimica Acta 223, 175-197.

Galli, A., Grassi, D., Sartori, G., Gianola, O., Burg, J.-P., Schmidt, M.W., 2019. Jurassic carbonatite and alkaline magmatism in the Ivrea zone (European Alps) related to the breakup of Pangea. Geology 47, 1–4, https://doi.org/10.1130/G45678.1.

Garuti, G., Bea, F., Zaccarini, F., Montero, P., 2001. Age, geochemistry and petrogenesis of the ultramafic pipes in the Ivrea Zone, NW Italy. Journal of Petrology 42, 433–457.

Giovanardi, T., Morishita, T., Zanetti, A., Mazzucchelli, M., Vannucci, R., 2013. Igneous sapphirine as a product of melt-peridotite interactions in the Finero Phlogopite-Peridotite Massif, Western Italian Alps. European Journal of Mineralogy 25, 17-31.

Giovanardi, T., Mazzucchelli, M., Zanetti, A., Langone, A., Tiepolo, M., Cipriani, A., 2014. Occurrence of Phlogopite in the Finero Mafic Layered Complex. Central European Journal of Geosciences 6 (4), 588-613.

Giovanardi, T., Girardi, V.A.V., Correia, C.T., Sinigoi, S., Tassinari, C.C.G., Mazzucchelli, M., 2017. The growth and contamination mechanism of the Cana Brava layered mafic-ultramafic complex: new field and geochemical evidences. Mineralogy and Petrology 111, 291-314.

Giovanardi, T., Freddo, I., Mazzucchelli, M., 2018. Filling the Gap in the Classification of Phlogopite-Bearing Ultramafic Rocks. The Journal of Geology 126, 361–370.

Grieco, G., Ferrario, A., von Quadt, A., Köppel, V., Mathez, A., 2001. The zircon-bearing chromitites of the phlogopite peridotite of Finero (Ivrea Zone, Southern Alps): evidence and geochronology of a metasomatized mantle slab. Journal of Petrology 42/1, 89-101.

Grieco, G., Ferrario, A., Mathez, E.A., 2004. The effect of metasomatism on the Cr-PGE mineralization in the Finero Complex, Ivrea Zone, Southern Alps. Ore Geology Reviews 24, 299-314.

Griffin, W.L., O'Reilly, S.Y., 1986. Mantle-derived sapphirine. Mineralogical Magazine 50, 635-640.

Griffin, W.L., Powell, W.J., Pearson, N.J., O'Reilly, S.Y., 2008. GLITTER: data reduction software for laser ablation ICPBMS. In: Sylvester P. (Ed.), Laser Ablation ICP–MS in the Earth Sciences:

Current Practices and Outstanding Issues. Mineralogical Association of Canada Short Course Series 40, 308-311.

Hartmann, G., Wedepohl, K.H., 1993. The composition of peridotite tectonites from the Ivrea Complex, northern Italy: Residues from melt extraction. Geochimica et Cosmochimica Acta 57, 1761-1782.

Higgins, J.B., Ribbe, R.H., Herd, R.K., 1979. Sapphirine I. Crystal chemical contributions. Contribution to Mineralogy and Petrology 68, 349-356.

Holland, T., Blundy, J., 1994. Non-ideal interactions in calcic amphiboles and their bearing on amphibole-plagioclase thermometry. Contributions to Mineralogy and Petrology 116, 433-447.

Ionov, D.A., Bodinier, J.-L., Mukasa, S.B., Zanetti, A., 2002. Mechanisms and sources of mantle metasomatism: major and trace element compositions of peridotite xenoliths from Spitsbergen in the context of numerical modelling. Journal of Petrology 43, 1-41.

Janin, M., Hémond, C., Maia, M., Nonnotte, P., Ponzevera, E., Johnson, K.T.M., 2012. The Amsterdam–St. Paul Plateau: A complex hot spot/DUPAL-flavored MORB interaction. Geochemistry Geophysics Geosystems 13-9, 10.1029/2012GC004165.

Langone, A., Padrón-Navarta, J. A., Ji, W.-Q., Zanetti, A., Mazzucchelli, M., Tiepolo, M., Giovanardi, T., Bonazzi, M., 2017. Ductile-brittle deformation effects on crystal-chemistry and U-Pb ages of magmatic and metasomatic zircons from a dyke of the Finero Mafic Complex (Ivrea-Verbano Zone, Italian Alps). Lithos 284-285, 493-511.

Langone, A., Zanetti, A., Daczko, N.R., Piazolo, S., Tiepolo, M., Mazzucchelli, M., 2018. Zircon U-Pb dating of a lower crustal shear zone: A case study from the northern sector of the Ivrea-Verbano Zone (Val Cannobina, Italy). Tectonics 37, 322–342.

Lensch, G., 1968. Die Ultramafitite der Zone von Ivrea und ihre geologische Interpretation. Schweizerische Mineralogische Petrographische Mitteilung 48, 91-102.

Liu, T.C., Presnall, D.C., 1990. Liquidus phase relationships on the join anorthite-forsterite-quartz at 20 kbar with applications to basalt petrogenesis and igneous sapphirine. Contributions to Mineralogy and Petrology 104, 735-742.

Liu, T.C., Presnall, D.C., 2000. Liquidus phase relations in the system CaO-MgO-Al2O3-SiO2 at 2.0 GPa: applications to basalt fractionation, eclogites, and igneous sapphirine. Journal of Petrology 41, 3-20.

Locmelis, M., Fiorentini, M.L., Rushmer, T., Arevalo Jr, R., Adam, J., Denyszyn, S.W., 2016. Sulfur and metal fertilization of the lower continental crust. Lithos 244, 74-93.

Lu, M., Hofmann, A.W., Mazzucchelli, M., Rivalenti, G., 1997a. The mafic-ultramafic complex near Finero (Ivrea-Verbano zone), I. Chemistry of MORB-like magmas. Chemical Geology 140, 207-222.

Lu, M., Hofmann, A.W., Mazzucchelli, M., Rivalenti, G., 1997b. The mafic-ultramafic complex near Finero (Ivrea-Verbano zone), II. Geochronology and isotope geochemistry. Chemical Geology 140, 223-235.

Lyubetskaya, T., Korenaga, J., 2007. Chemical composition of Earth's primitive mantle and its variance: 1. Method and results. Journal of Geophysical Research 112, B03211.

Malitch, K.N., Belousova, E.A., Griffin, W.L., Badanina, I.Yu., Knauf, V.V., O’Reilly, S.Y., Pearson, N.J., 2017. Laurite and zircon from the Finero chromitites (Italy): New insights into evolution of the subcontinental mantle: Ore Geology Reviews 90, 210–225.

Matsumoto, T., Morishita, T., Masuda, J., Fujioka, T., Takebe, M., Yamamoto, K., Arai, S., 2005. Noble gases in the Finero Phlogopite–Peridotites, ItalianWestern Alps. Earth and Planetary Science Letters 238, 130-145.

Matysiak, A.K., Trepmann, C.A., 2015. The deformation record of olivine in mylonitic peridotites from the Finero Complex, Ivrea Zone: Separate deformation cycles during exhumation. Tectonics 34, 2514-2533.

Mazzucchelli, M., Rivalenti, G., Piccirillo, E.M., Girardi, V.A.V., Civetta, L., Petrini, R., 1995. Petrology of the Proterozoic mafic dyke swarms of Uruguay and constraints on their mantle source composition.Precambrian Research 74, 177-194.

Mazzucchelli, M., Rivalenti, G., Brunelli, D., Zanetti, A., Boari, E., 2009. Formation of highly refractory dunite by focused percolation of pyroxenite-derived melt in the Balmuccia peridotite Massif (Italy). Journal of Petrology 50, 1205-1233.

Mazzucchelli, M., Zanetti, A., Rivalenti, G., Vannucci, R., Correia, C.T., Tassinari, C.C.G., 2010. Age and geochemistry of mantle peridotites and diorite dykes from the Baldissero body: Insights into the Paleozoic-Mesozoic evolution of the Southern Alps. Lithos 119, 485-500.

Mazzucchelli, M., Quick, J.E., Sinigoi, S., Zanetti, A., Giovanardi, T., 2014. Igneous evolutions across the Ivrea crustal section: The Permian Sesia Magmatic System and the Triassic Finero intrusion and mantle. Geological Filed Trips 6 (2.2), 1-98.

Mazzucchelli, M., Cipriani, A., Hémond, C., Zanetti, A., Bertotto, G.W., Cingolani, C.A., 2016. Origin of the DUPAL anomaly in mantle xenoliths of Patagonia (Argentina) and geodynamic consequences. Lithos 248-251, 257-271.

McDonough, W.F., Sun, S.-s., 1995. The composition of the Earth. Chemical Geology 120, 223-253.

Milholland, C.S., Presnall, D.C., 1998. Liquidus phase relations in the CaO-MgO-Al2O3-SiO2 system at 3.0 GPa: the Aluminous pyroxene thermal divide and high-pressure fractionation of picritic and komatiitic magmas. Journal of Petrology 39, 3-27.

Morishita, T., Arai, S., Tamura, A, 2003. Petrology of an apatite-rich layer in the Finero phlogopite–peridotite, Italian Western Alps; implications for evolution of a metasomatising agent. Lithos 69, 37-49.

Morishita, T., Hattori, K.H., Terada, K., Matsumoto, T., Yamamoto, K., Takebe, M., Ishida, Y., Tamura, A., Arai, S., 2008. Geochemistry of apatite-rich layers in the Finero phlogopite–peridotite massif (Italian Western Alps) and ion microprobe dating of apatite. Chemical Geology, 251 99-111.

Mukasa, S.B., Shervais, J.W., 1999. Growth of subcontinental lithosphere: evidence from repeated dike injections in the Balmuccia lherzolite massif, Italian Alps. Lithos 48, 287-316

Obermiller, W.A., 1994. Chemical and isotopic variations in the Balmuccia, Baldissero and Finero peridotite massifs (Ivrea-Zone, N-Italy). Unpublished PhD thesis, Johannes Gutenberg-Universität Mainz pp. 191.

Perinelli, C., Armienti, P., Dallai, L., 2011. Thermal evolution of the lithosphere in a rift environment as inferred from the geochemistry of mantle cumulates, Northen Victoria Land, Antarctica. Journal of Petrology 52, 665-690.

Petri, B., Duretza, T., Mohn, G., Schmalholz, S.M., Karner, G.D., Müntener, O., 2019. Thinning mechanisms of heterogeneous continental lithosphere. Earth and Planetary Science Letters 512, 147-162.

Piccardo, G.B., Zanetti, Z., Müntener, O., 2007. Melt/peridotite interaction in the Southern Lanzo peridotite: field, textural and geochemical evidence. Lithos 94, 181-209.

Polat, A., Frei, R.,. Longstaffe, F.J., Thorkelson, D.J., Friedman, E., 2018. Petrology and geochemistry of the Tasse mantle xenoliths of the Canadian Cordillera: A record of Archean to Quaternary mantle growth, metasomatism, removal, and melting. Tectonophysics 737, 1-26.

Ponce, A.D., Bertotto, G.W., Zanetti, A., Brunelli, D., Giovanardi, T., Aragón, E., Bernardi, M.I., Hémond, C., Mazzucchelli, M., 2015. Short-scale variability of the SCLM beneath the extra-Andean back-arc (Paso de Indios, Argentina): evidence from spinel-facies mantle xenoliths. Open Geosciences 7, 362–385.

Princivalle, F., DeMin, A., Lenaz, D., Scarbolo, M., Zanetti, A., 2014. Ultramafic xenoliths from Damaping (Hannuoba region, NE-China): Petrogenetic implications from crystal chemistry of pyroxenes, olivine and Cr-spinel and trace element content of clinopyroxene. Lithos 188, 3-14.

Quick, J.E., Sinigoi, S., Mayer, A., 1995. Emplacement of mantle peridotite in the lower continental crust, Ivrea-Verbano Zone, northwest Italy. Geology 23, 739-742.

Raffone, N., Le Fèvre, B. L., Ottolini, L., Vannucci, R., Zanetti, A., 2006. Light-lithophile element metasomatism of Finero peridotite (W Alps): A secondary-ion mass spectrometry study. Microchimica Acta 155, 251-255.

Ridolfi, F., Zanetti, A., Renzulli, A., Perugini, D., Holtz, F., Oberti, R., 2018. AMFORM, a new mass-based model for the calculation of the unit formula of amphiboles from electron microprobe analyses. American Mineralogist 103, 1112-1125.

Rivalenti, G., Mazzucchelli, M., Molesini, M., Petrini, R., Girardi, V.A.V., Bossi, J., Campal, N., 1995. Petrology of late proterozoic mafic dikes in the Nico Perez region, central Uruguay. Mineralogy and Petrology 55, 239-263.

Rivalenti, G., Mazzucchelli, M., Zanetti, A., Vannucci, R., Bollinger, C., Hémond, C., Bertotto, G.W., 2007a. Xenoliths from Cerro de los Chenques (Patagonia): An example of slab-related metasomatism in the backarc lithospheric mantle, Lithos 99, 45-67.

Rivalenti, G., Zanetti, A., Girardi, V.A.V., Mazzucchelli, M., Tassinari, C.C.G., Bertotto, G.W., 2007b. The effect of the Fernando de Noronha plume on the mantle lithosphere in north-eastern Brazil. Lithos 94, 111-131.

Rocco, I., Zanetti, A., Melluso, L., Morra, V., 2017. Ancient-depleted and enriched mantle lithosphere domains in northern Madagascar: geochemical and isotopic evidence from spinel-to-plagioclase-bearing ultramafic xenoliths. Chemical Geology 466, 70-85.

Rollinson, H., 1993. Using geochemical data: evaluation, presentation interpretation. Longman Group UK Ltd, 1994 reprinted, pp. 352.

Sapienza, G.T., Scambelluri, M., Braga, R., 2009. Dolomite-bearing orogenic garnet peridotites witness fluid-mediated carbonrecycling in a mantle wedge (Ulten Zone, Eastern Alps, Italy). Contributions to Mineralogy and Petrology 158, 401-420.

Sato, K., Miyamoto, T., Kawasaki, T., 2006. Experimental calibration of sapphirine-spinel Fe^{2+}-Mg exchange thermometer: implication for constraints on P-T condition of Howard Hills, Napier Complex, East Antarctica. Gondwana Research 9, 398-408.

Schaltegger, U., Ulianov, A., Müntener, O., Ovtcharova, M., Peytcheva, I., Vonlanthen, P., Vennemann, T., Antognini, M., Girlanda, F., 2015. Megacrystic zircon with planar fractures in miaskite–type nepheline pegmatites formed at high pressures in the lower crust (Ivrea Zone, southern Alps, Switzerland). American Mineralogist 100, 83-94.

Schmid, S.M., Bernoulli, D., Fügenschuh, B., Matenco, L., Schefer, S., Schuster, R., Tischler, M., Ustaszewsk, K., 2008. The Alpine-Carpathian-Dinaridic orogenic system: correlation and evolution of tectonic units. Swiss Journal of Geosciences 101, 139-183.

Schulmann, K., Lexa, O., Janoušek, V., Lardeaux, J.M., Edel, J.B., 2014. Anatomy of a diffuse cryptic suture zone: An example from the Bohemian Massif, European Variscides. Geology 42, 275-278.

Seitz, H.M., Woodland, A.B., 2000. The distribution of lithiumin peridotitic and pyroxenitic mantle lithologies - an indicator of magmatic and metasomatic processes. Chemical Geology 166, 47–64.

Selverstone, J., Sharp, Z.D., 2011. Chlorine isotope evidence for multicomponent mantle metasomatism in the Ivrea Zone. Earth and Planetary Science Letters 310, 429-440.

Shervais, J.W., Mukasa, S.B., 1991. The Balmuccia orogenic lherzolite massif, Italy. Journal of Petrology, Special Lherzolite issue, 155-174.

Siena, F., Coltorti, M., 1989. The petrogenesis of a hydrated mafic - ultramafic complex and the role of amphibole fractionation at Finero (Italian Western Alps). Neues Jahrbuch für Mineralogie 6, 255-274.

Sills, J.D., Ackermand, D., Herd, R.K., Windley, B.F., 1983. Bulk composition and mineral parageneses of sapphirine-bearing rocks along a gabbro-lherzolite contact at Finero, Ivrea Zone, N Italy. Journal of Metamorphic Geology 1, 337-351.

Stälhe, V., Frenzel, G., Kober, B., Michard, A., Puchelt, H., Schneider, W., 1990. Zircon syenite pegmatites in the Finero peridotite (Ivrea Zone): evidence for a syenite from a mantle source. Earth and Planetary Science Letters 101, 196-205.

Stähle, V., Frenzel, G., Hess, J. C., Saupé, F., Schmidt, S. Th., Schneider, W., 2001. Permian metabasalt and Triassic alkaline dykes in the Northern Ivrea Zone: clues to the post-Variscan geodynamic evolution of the Southern Alps. Schweizerische Mineralogische und Petrographische Mitteilungen 81, 1-21.

Tiepolo, M., Oberti, R., Zanetti, A., Vannucci, R, Foley, S.F., 2007. Trace-Element partitioning between Amphibole and silicate melt. Reviews in Mineralogy and Geochemistry 67, 417-452.

Tommasi, A., Langone, A., Padrón-Navarta, J. A., Zanetti, A., Vauchez, A., 2017. Hydrous melts weaken the mantle, crystallization of pargasite and phlogopite does not: Insights from a petrostructural study of the Finero peridotites, Southern Alps. Earth and Planetary Science Letters 477, 59–72.

Voshage, H., Hunziker, J.C., Hofmann, A.W., Zingg, A., 1987. A Nd and Sr isotopic study of the Ivrea zone, Southern Alps, N-Italy. Contributions to Mineralogy and Petrology 97, 31–42.

Voshage, H., Sinigoi, S., Mazzucchelli, M., Demarchi, G., Rivalenti, G., Hofmann, A.W., 1988. Isotopic constraints on the origin of ultramafic and mafic dikes in the Balmuccia peridotite (Ivrea Zone). Contributions to Mineralogy and Petrology 100 (3), 261–267.

Workman, R.K., Hart, S.R., 2005) Major and trace element composition of the depleted MORB mantle (DMM). Earth Planetary Science Letter 231, 53–72.

Zaccarini, F., Stumpfl, E.F., Garuti, G., 2004. Zirconolite and Zr–Th–U minerals in chromitites of the Finero complex, Western Alps, Italy: evidence for carbonatite type metasomatism in a subcontinental mantle plume. The Canadian Mineralogist 42, 1825–1845.

Zanetti, A., Mazzucchelli, M., Rivalenti, G., Vannucci, R., 1999. The Finero phlogopite-peridotite massif: an example of subduction-related metasomatism. Contributions to Mineralogy and Petrology 134, 107-122.

Zanetti, A., Mazzucchelli, M., Sinigoi, S., Giovanardi, T., Peressini, G., Fanning, M., 2013. Insights into the Melt-Lower Crust Interplay in Subduction-related Setting and the Mesozoic Geodynamic

Evolution of the Southern Alps: evidence from the Finero Mafic Complex (Ivrea-Verbano Zone). Journal of Petrology 54, 2235-2265.

Zanetti, A., Mazzucchelli, M., Sinigoi, S., Giovanardi, T., Peressini, G., Fanning, M., 2014. Erratum Insights into the Melt-Lower Crust Interplay in Subduction-related Setting and the Mesozoic Geodynamic Evolution of the Southern Alps: evidence from the Finero Mafic Complex (Ivrea-Verbano Zone). Journal of Petrology 55, 1239-1240.

Zanetti, A., Giovanardi, T., Langone, A., Tiepolo, M., Wu, F.-Y., Dallai, L., Mazzucchelli, M., 2016. Origin and age of zircon-bearing chromitite layers from the Finero phlogopite peridotite (Ivrea–Verbano Zone, Western Alps) and geodynamic consequences. Lithos 262, 58-74.

Figure captions

Figure 1: Geological map of the Finero area, modified after Mazzucchelli et al. (2014).

Figure 2: A) Sample FI09C06 crosscutting the host harzburgite foliation. The centre of the dyke is formed by the Leucocratic Zone, whereas the melanocratic zones (i.e. the Orthopyroxene Zone, Early Amphibole Zone, and Late Amphibole Zone) are indistinguishable; B) phlogopite vein cutting the Orthopyroxene Zone; C–F) occurrences of sapphirine in sample FI09C06 (C and D) and sample FI9664 (E and F). The figures show the increase of sapphirine size, from μm (C) to mm (D and E) and cm scale (F).

Figure 3: Primitive mantle (PM)-normalised bulk rock trace elemental patterns of a gabbroic dyke and host harzburgite. PM values are from McDonough and Sun (1995). Literature values from the harzburgite-pyroxenite association of (1) Hartmann and Wedephol (1993) and nepheline-bearing hornblende syenitic dykes of (2) Stähle et al. (2001) are reported for comparison.

Figure 4: Orthopyroxene major elemental contents from host harzburgites, dykes, and literature data. Plotted literature data are the harzburgite-pyroxenite association orthopyroxene from (1) Zanetti et al. (1999) and orthopyroxene from sapphirine-bearing rock from the Mafic Complex from (2) Sills et al. (1983).

Figure 5: Phlogopite major elemental contents from host harzburgites, dykes, and literature data. Plotted literature data are: harzburgite-pyroxenite association phlogopite from (1) Zanetti et al. (1999).

Figure 6: Amphibole major elemental contents from host harzburgites, dykes, and literature data. Plotted literature data are: harzburgite-pyroxenite association amphibole compositions from (1) Zanetti et al. (1999) and (2) Morishita et al. (2008), amphibole from apatite-rich veins in the FPP

from (1) Zanetti et al. (1999) and (2) Morishita et al. (2008), and amphibole from sapphirine-bearing rock from the Mafic Complex from (3) Sills et al. (1983).

Figure 7: Sapphirine compositions plotted in the (MgO + FeO)–(Cr_2O_3 + Fe_2O_3 + Al_2O_3)–SiO_2 diagram (mol. %). Literature data are from sapphirine of the Finero Mafic Complex (Sills et al., 1983) and sapphirine 1 of Higgins et al. (1979).

Figure 8: REE patterns of clinopyroxene and amphibole from the gabbroic dykes and the respective host rocks divided for samples and position. Values are normalised to Chrondrite-I (CI, values from Lyubetskaya and Korenaga (2007); $\delta^{18}O$ values (normalised to SMOW) from phases of sample FI09C06 are reported near the REE patterns according to their positions in the sample.

Figure 9: PM-normalised trace elemental patterns of clinopyroxene from host harzburgite. PM values are from McDonough and Sun (1995). Plotted literature data are: clinopyroxene and amphibole average compositions from the harzburgite-pyroxenite association from (1) Zanetti et al. (1999) and (2) Morishita et al. (2008), clinopyroxene and amphibole average from apatite-rich veins in the FPP from (1) Zanetti et al. (1999) and (2) Morishita et al. (2008), reported as apatite veins.

Figure 10: PM-normalised trace elemental patterns of amphiboles from gabbroic dyke and host harzburgite. PM values are from McDonough and Sun (1995).

Figure 11: $\delta^{18}O$ normalised to SMOW. Values from literature are the field of mantle and variation of MORB from Rollinson (1993), and mantle ultramafics and mantle-derived melts (*) from Bindeman (2008). Finero literature data are reported from the harzburgite-pyroxenite association of Hartmann and Wedephol (1993) and Selverstone and Sharp (2011) and from chromitite in dunite bodies from Zanetti et al. (2016).

Figure 12: ^{143}Nd/^{144}Nd vs ^{87}Sr/^{86}Sr recalculated at 225 Ma for amphibole and plagioclase from the various zones of sample FI09C06 (host and dyke): (1) amphibole data of the FPP from Obermiller (1994); (2) bulk rock data of the Finero Mafic Complex from Lu et al. (1997b); (3) data from an alkaline dyke in the FPP from Stähle et al. (1990); (4) data from an alkaline dyke in the FPP from Stähle et al. (2001); (5) amphibole and apatite data from discordant apatite-bearing veins in the FPP from Morishita et al. (2008); (6) Mesozoic shoshonitic magmatism (SS: silica saturated; US: undersaturated in silica) in the Predazzo area from Casetta et al. (2018a, b); Depleted MORB Mantel (DMM) from Workman and Hart (2005). The mixing model was calculated between the two end-members: the alkaline dyke S9 of Stähle et al. (1990) and the hosting peridotite FI09C06. Data for the melt in equilibrium with the alkaline dyke S9 are: ^{143}Nd/^{144}Nd = 0.512607, ^{87}Sr/^{86}Sr = 0.703720 (from Stähle et al., 1990; recalculated at 225 Ma), Nd = 8.333 ppm, and Sr = 830 ppm (calculated from LA-ICP-MS plagioclase analysis of albitite dykes similar to the dyke of Stähle et al., 1990, using the K_d of Dohmen and Blundy, 2014; average Nd = 0.25 ppm, Sr = 5810 ppm). Data for the melt in equilibrium with the host FPP peridotite are ^{143}Nd/^{144}Nd = 0.512130, ^{87}Sr/^{86}Sr = 0.708501 (recalculated at 225 Ma), Nd = 67.5 ppm, and Sr = 909 ppm (calculated using the K_d of Ionov et al., 2002).

Figure 1

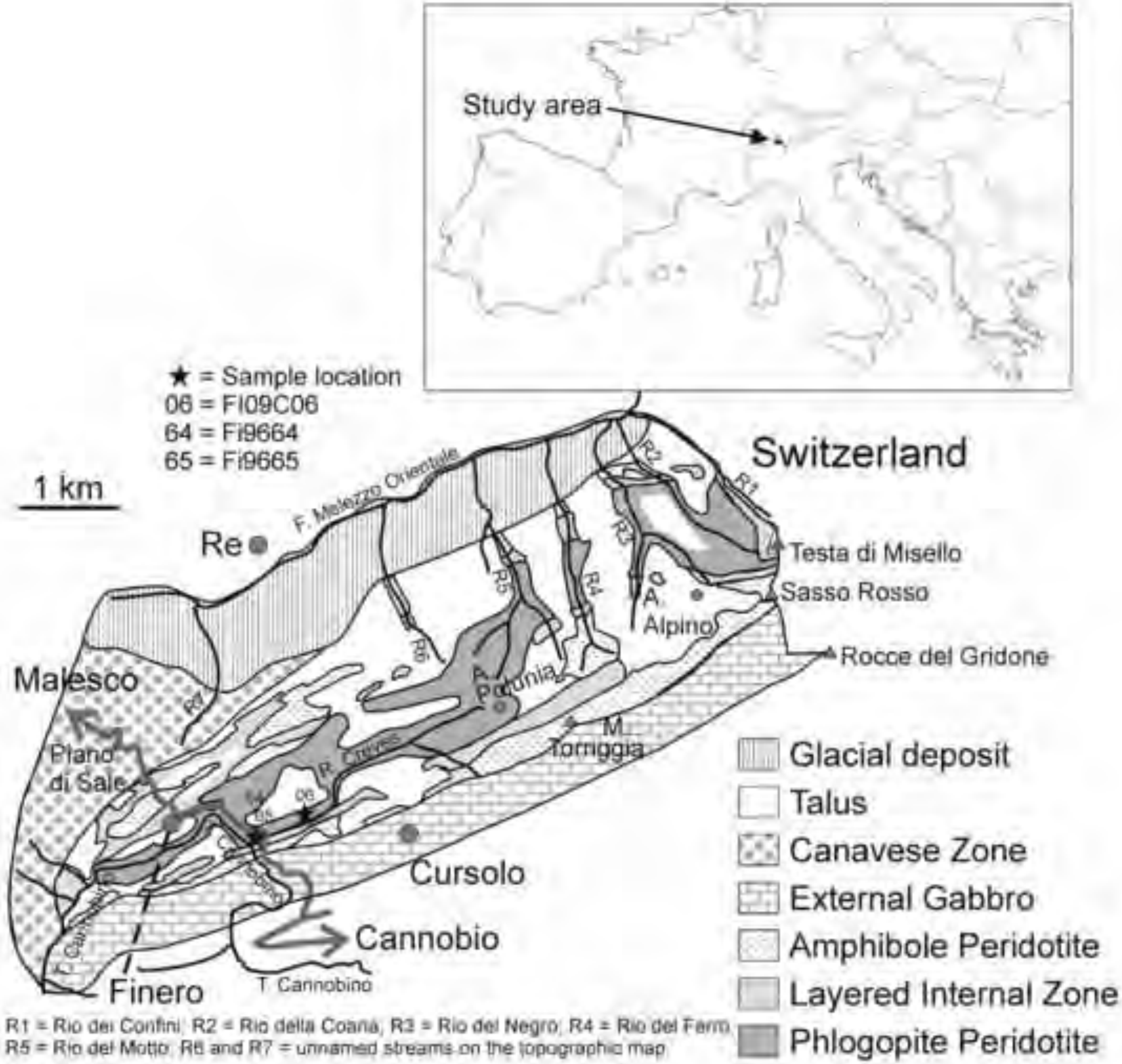
Study area
★ = Sample location
06 = FI09C06
64 = Fi9664
65 = Fi9665
1 km
Switzerland
F. Melezzo Orientale
Re
R1
R2
R3
R4
R5
R6
R7
Testa di Misello
Sasso Rosso
A. Alpino
Rocce del Gridone
Malesco
A. Pozunia
M. Torriggia
Piano di Sale
R. Creves
64
65
06
Cursolo
Cannobio
Finero
T. Cannobino
F. Cannobino
Glacial deposit
Talus
Canavese Zone
External Gabbro
Amphibole Peridotite
Layered Internal Zone
Phlogopite Peridotite
R1 = Rio dei Confini; R2 = Rio della Coana; R3 = Rio del Negro; R4 = Rio del Ferro
R5 = Rio del Motto; R6 and R7 = unnamed streams on the topographic map

Figure 2

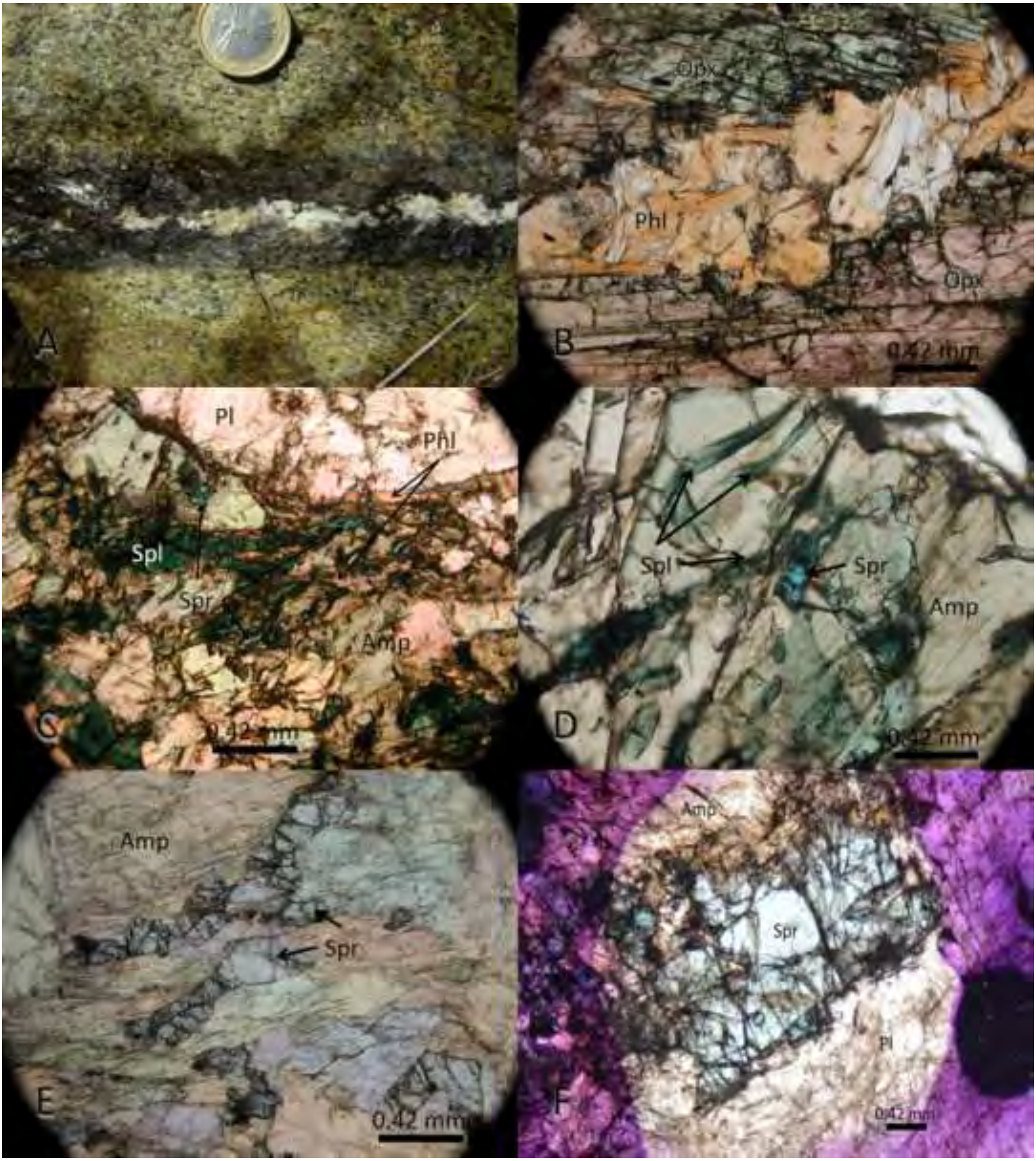
A
Opx
Phl
Opx
B
0.42 mm
Pl
Phl
Spl
Spr
Amp
C
0.42 mm
Spl
Spr
Amp
D
0.42 mm
Amp
Spr
E
0.42 mm
Amp
Spr
Pl
F
0.42 mm

Figure 3

Click here to download high resolution image

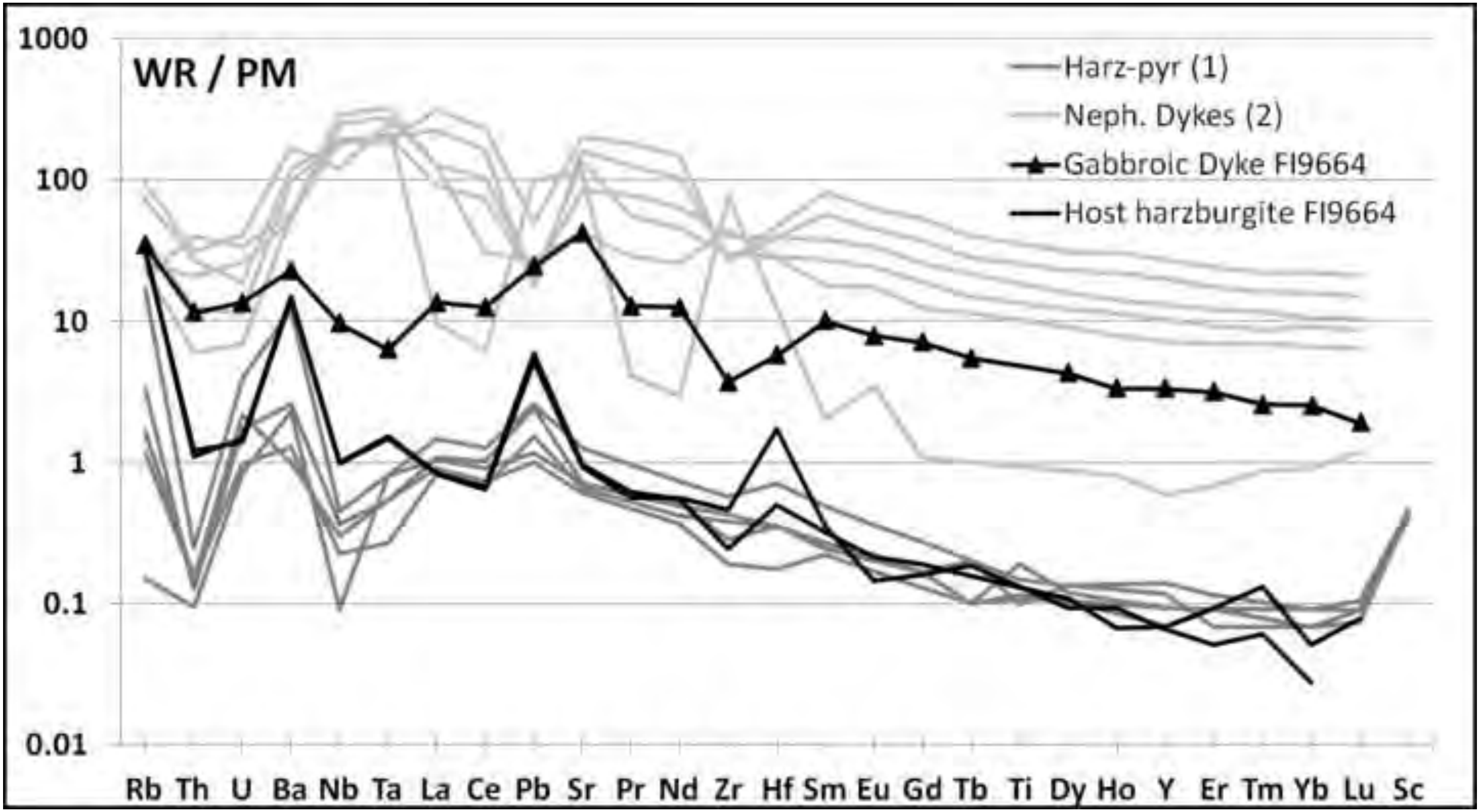

Figure 4

Click here to download high resolution image

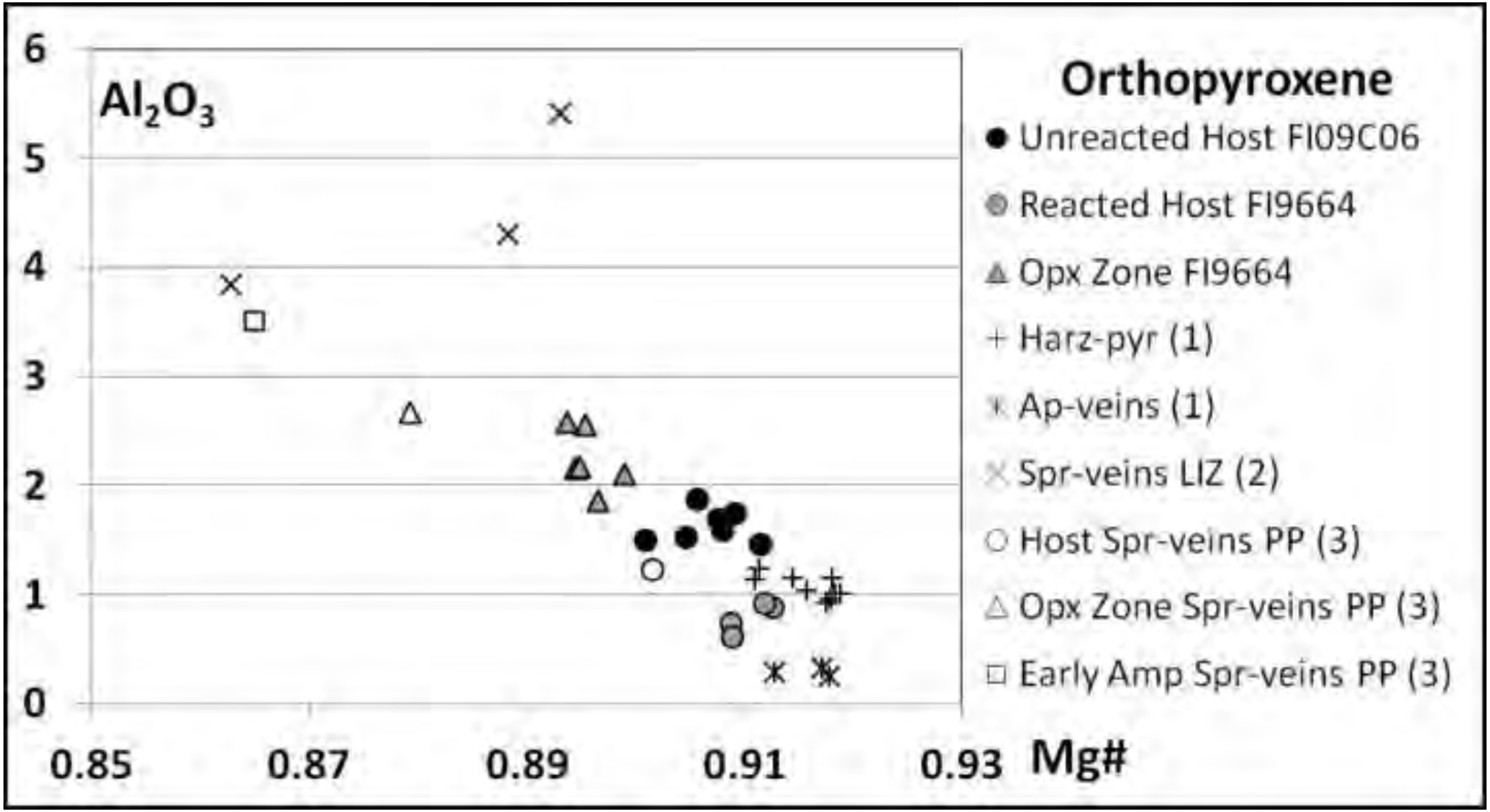

Figure 5

Click here to download high resolution image

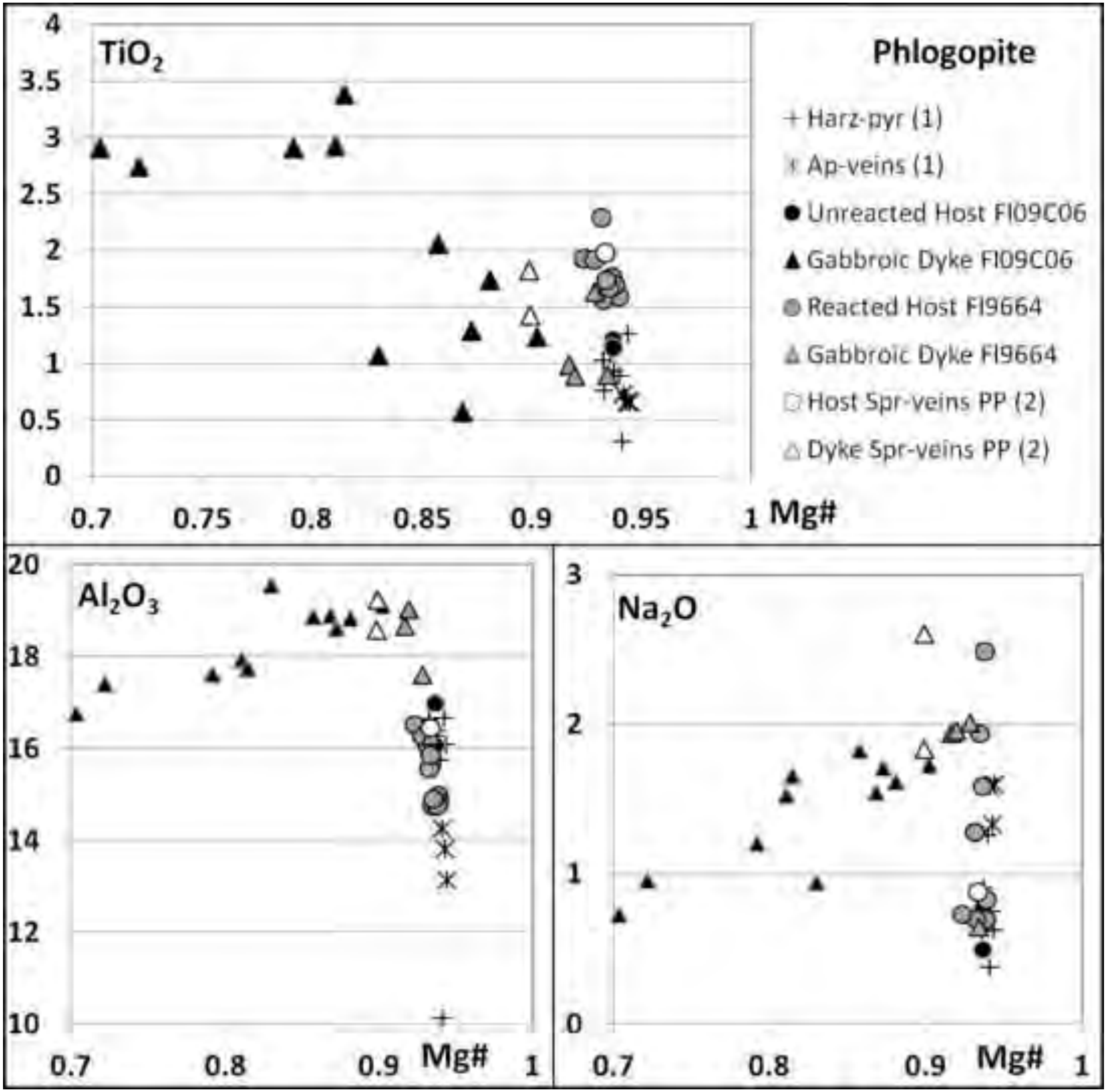

Figure 6

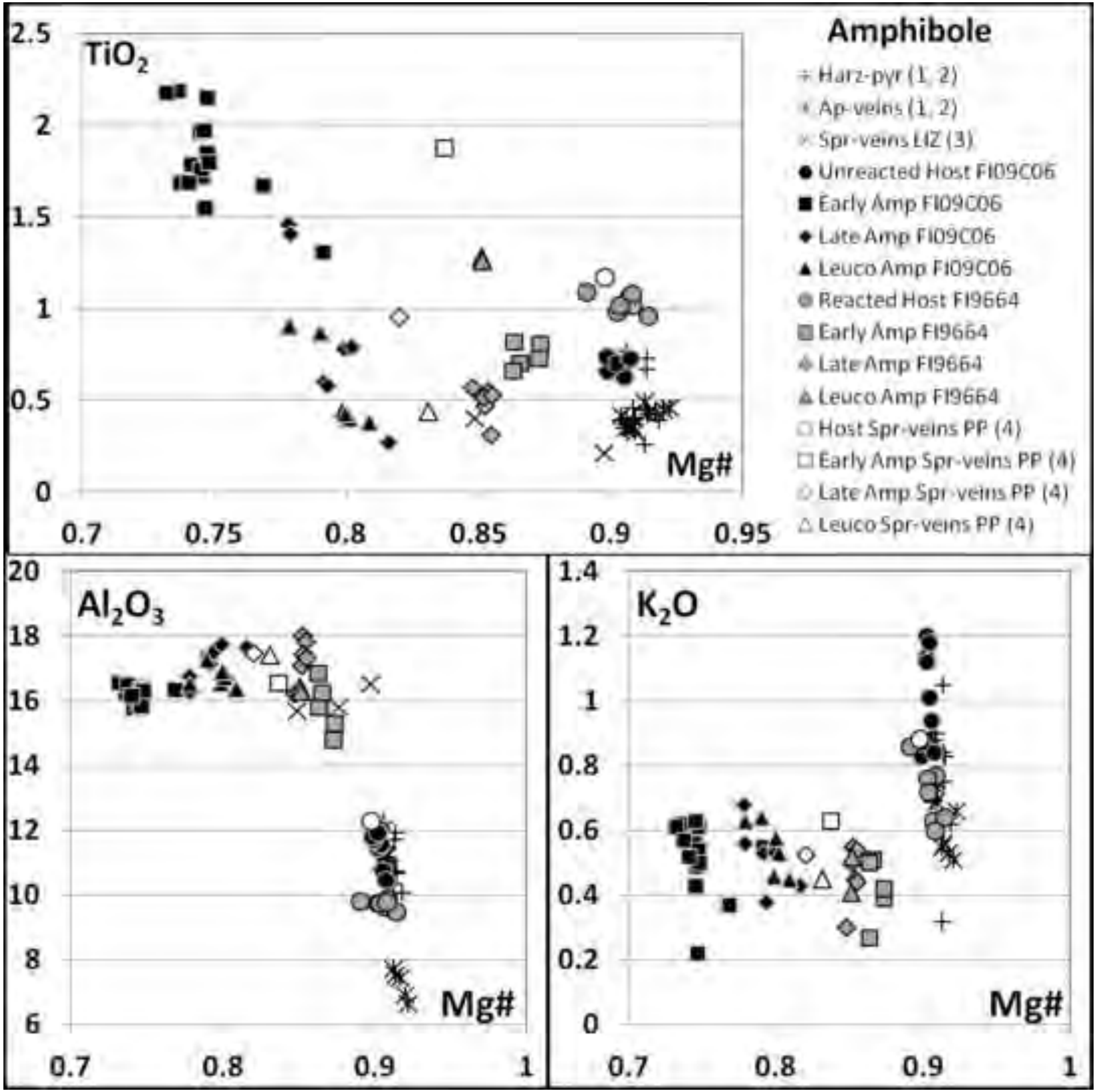
Amphibole
+ Harz-pyr (1, 2)
✱ Ap-veins (1, 2)
× Spr-veins LIZ (3)
● Unreacted Host FI09C06
■ Early Amp FI09C06
◆ Late Amp FI09C06
▲ Leuco Amp FI09C06
● Reacted Host FI9664
■ Early Amp FI9664
◆ Late Amp FI9664
▲ Leuco Amp FI9664
○ Host Spr-veins PP (4)
☐ Early Amp Spr-veins PP (4)
◇ Late Amp Spr-veins PP (4)
△ Leuco Spr-veins PP (4)
TiO$_2$
2.5
2
1.5
1
0.5
0
0.7
0.75
0.8
0.85
0.9
0.95
Mg#
Al$_2$O$_3$
20
18
16
14
12
10
8
6
0.7
0.8
0.9
1
Mg#
K$_2$O
1.4
1.2
1
0.8
0.6
0.4
0.2
0
0.7
0.8
0.9
1
Mg#

Figure 7

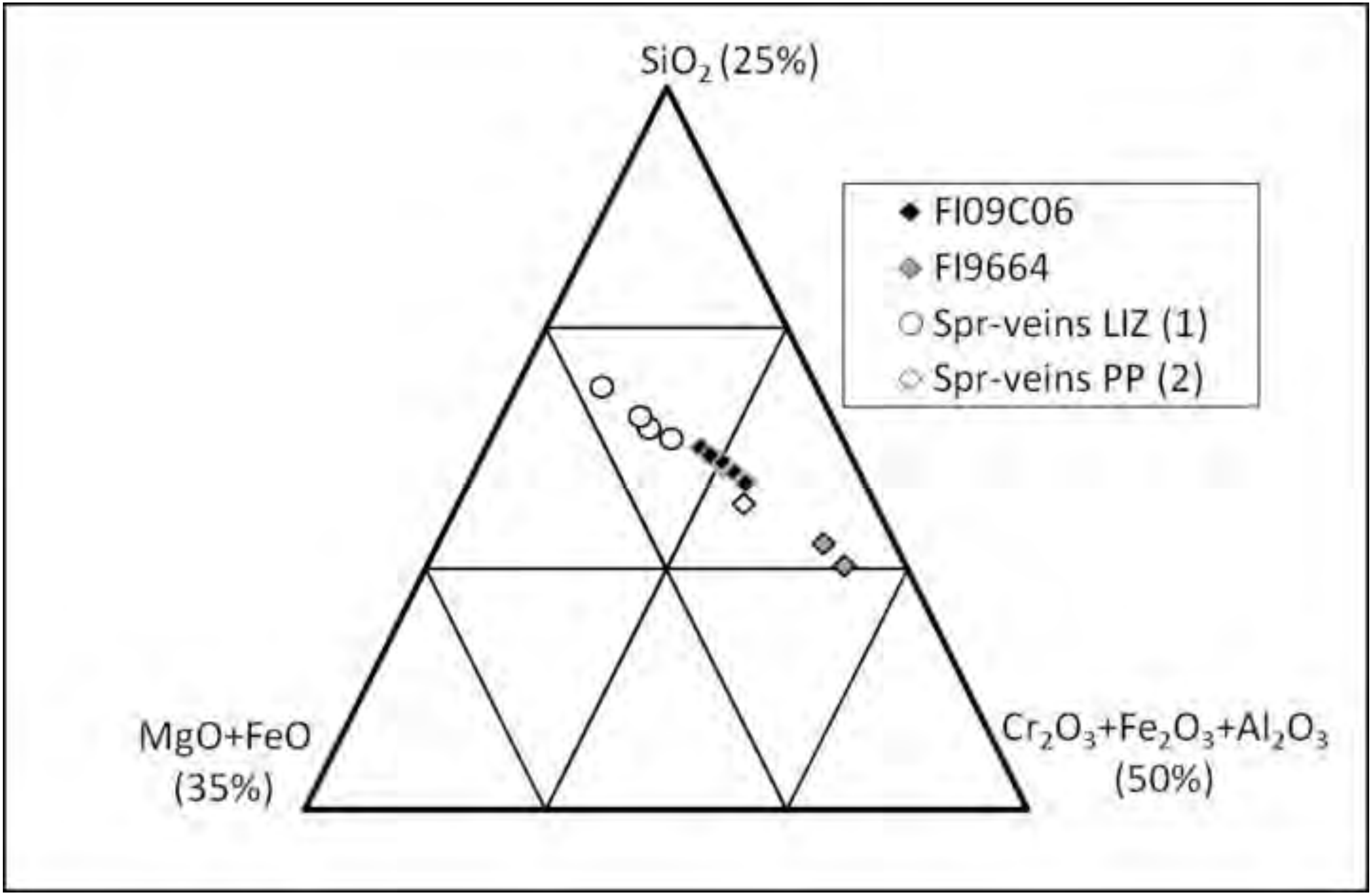
SiO_2 (25%)
MgO+FeO (35%)
$Cr_2O_3+Fe_2O_3+Al_2O_3$ (50%)
◆ FI09C06
◆ FI9664
○ Spr-veins LIZ (1)
◇ Spr-veins PP (2)

Figure 8

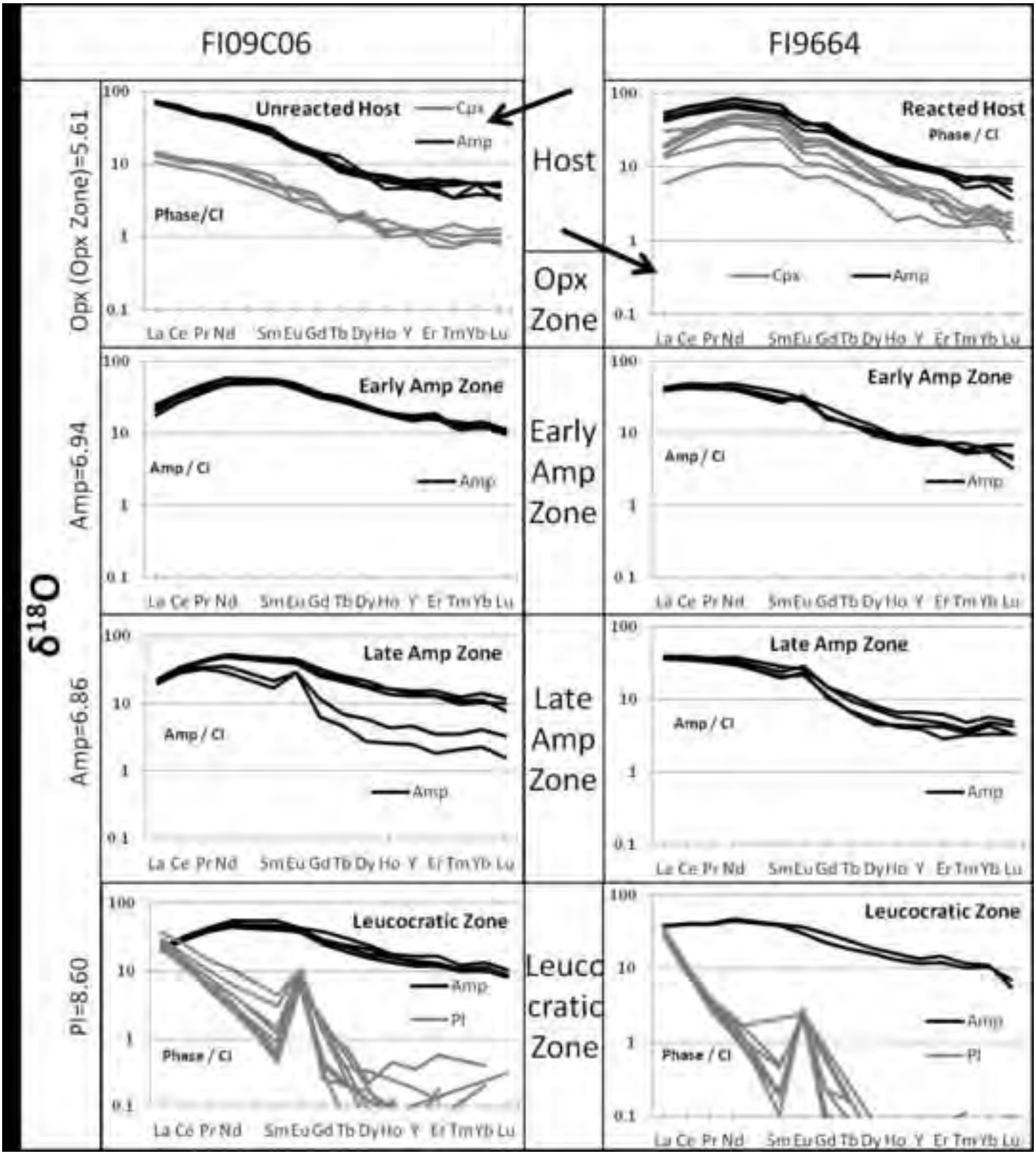
FI09C06
FI9664
δ18O
Opx (Opx Zone)=5.61
Amp=6.94
Amp=6.86
Pl=8.60
Host
Opx Zone
Early Amp Zone
Late Amp Zone
Leucc cratic Zone
Unreacted Host
Cpx
Amp
Phase/Cl
Reacted Host
Phase / Cl
Cpx
Amp
Early Amp Zone
Amp / Cl
Amp
Early Amp Zone
Amp / Cl
Amp
Late Amp Zone
Amp / Cl
Amp
Late Amp Zone
Amp / Cl
Amp
Leucocratic Zone
Amp
Pl
Phase / Cl
Leucocratic Zone
Amp
Pl
Phase / Cl
100
10
1
0.1
La Ce Pr Nd Sm Eu Gd Tb Dy Ho Y Er Tm Yb Lu

Figure 9

Click here to download high resolution image

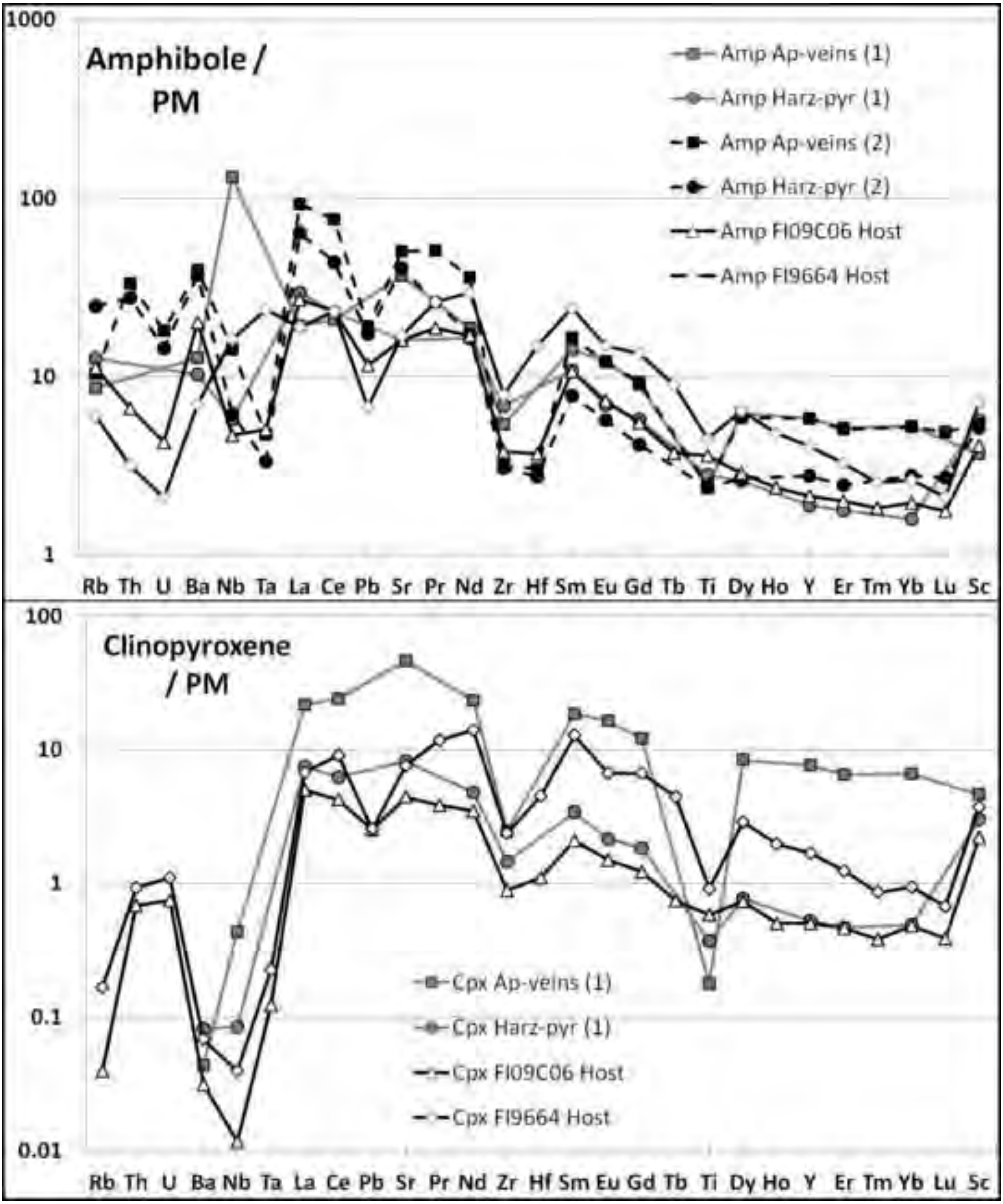

Figure 10

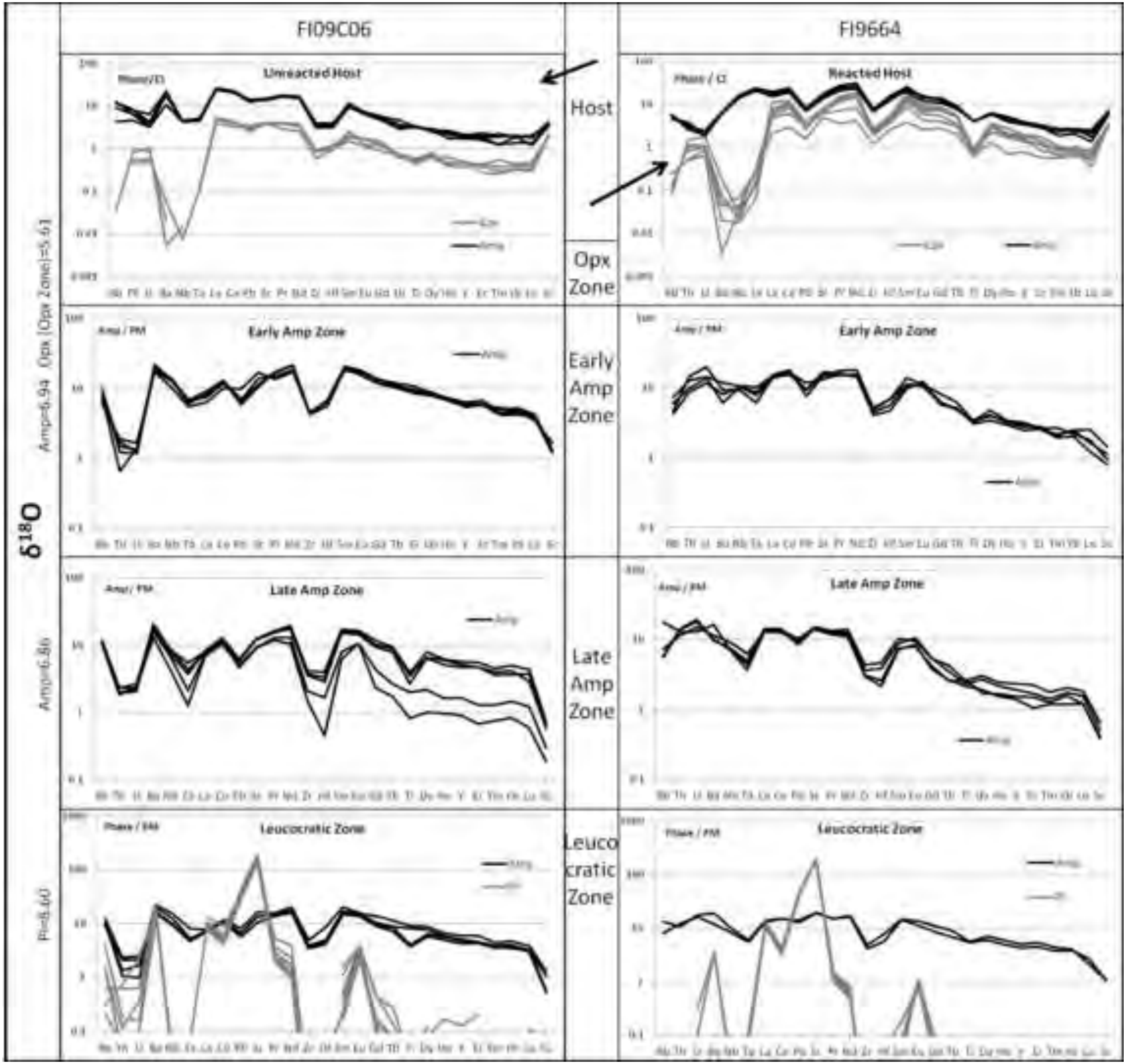
FI09C06
FI9664
Unreacted Host
Reacted Host
Host
Opx Zone
Early Amp Zone
Early Amp Zone
Early Amp Zone
Late Amp Zone
Late Amp Zone
Late Amp Zone
Leucocratic Zone
Leucocratic Zone
Leucocratic Zone
Amp / PM
Phase / PM
Amp
Pl
$\delta^{18}O$
Amp=6.94 Opx (Opx Zone)=5.61
Amp=6.86
Pl=8.60
100
10
1
0.1
0.01
0.001

Figure 11

Click here to download high resolution image

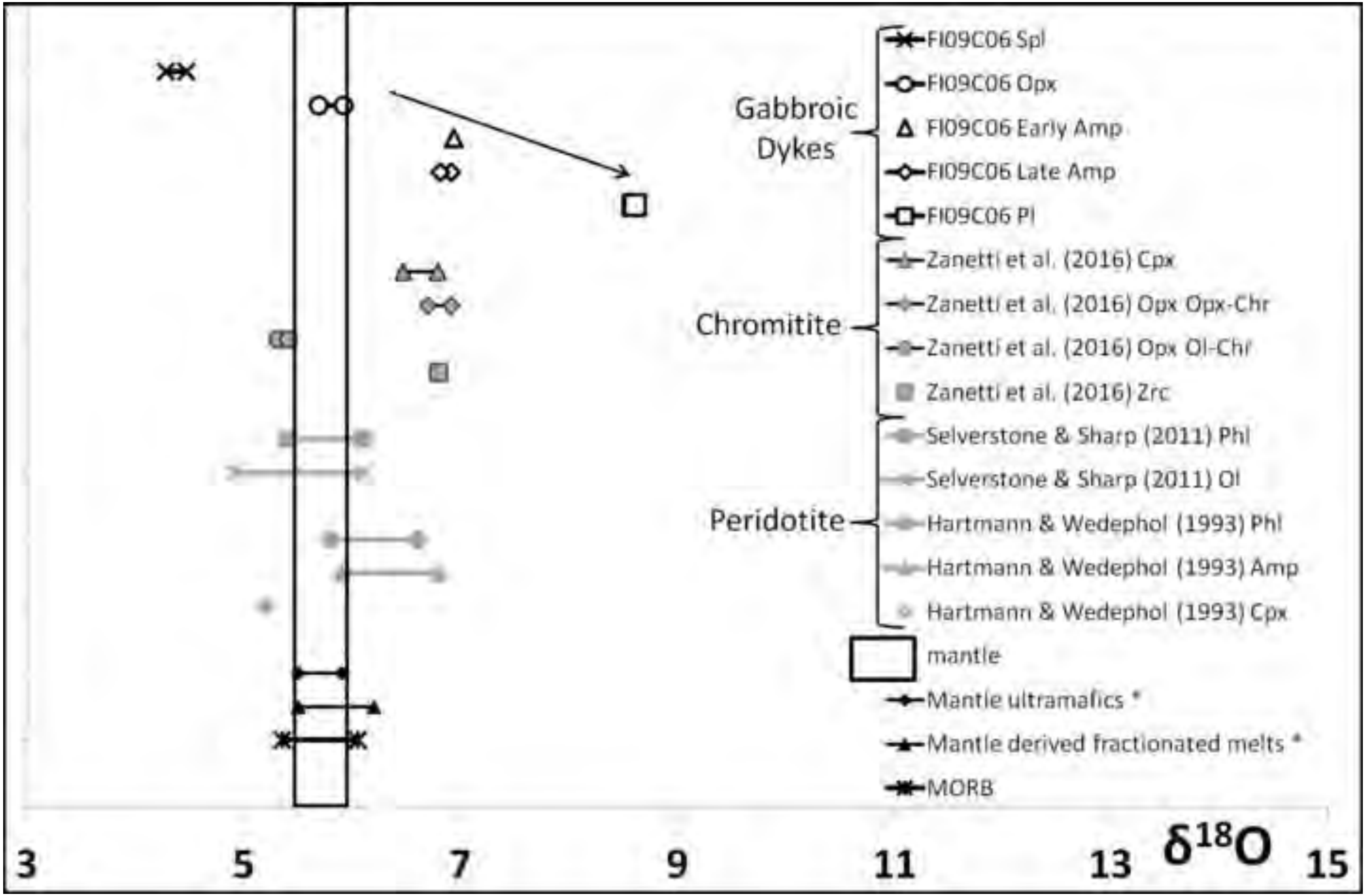

Figure 12

Click here to download high resolution image

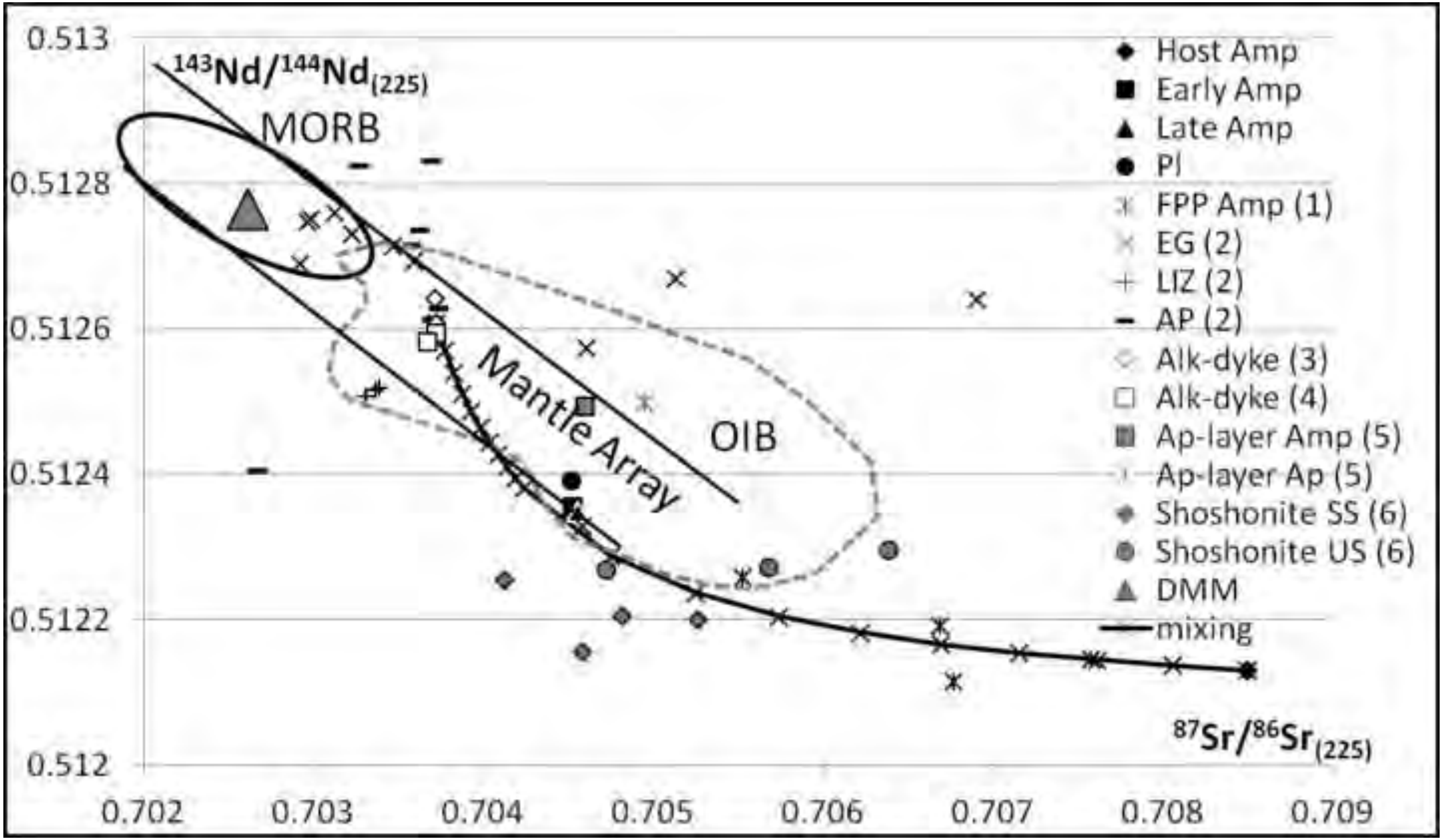

Table 1: O isotopic composition of minerals from the Spr-bearing gabbroic dykes.

Sample	**Phase**	**δ^{18}O**	**std. dev.**
FI09C06	Early Amp	6.94	0.00
FI09C06	Late Amp	6.86	0.05
FI09C06	Pl	8.60	0.01
FI09C06	Opx	5.81	0.11

Table 2: Sr and Nd isotopic composition of minerals from sample FI09C06 from the Spr-bearing gabbroic dykes and the host peridotite.

Rock	Phase	Rb	Sr	^{87}Sr/^{86}Sr	2SE	^{87}Rb/^{86}Sr	Nd	Sm	^{143}Nd/^{144}Nd	2SE	^{147}Sm/^{144}Nd
Host	Amp	6.5	281.2	0.708713	0.000008	0.066372	19.7	4.2	0.512317	0.000008	0.126796
Dyke	Early Amp	6.8	324.4	0.704722	0.000008	0.060834	24.8	8.1	0.512646	0.000008	0.197559
Dyke	Late Amp	8.6	189.5	0.704971	0.000008	0.131167	16.8	4.0	0.512559	0.000006	0.142593
Dyke	Pl	0.6	3109.7	0.704519	0.000008	0.000568	2.2	0.2	0.512482	0.000006	0.061238